Article

Developmental Cell

# APC Inhibits Ligand-Independent Wnt Signaling by the Clathrin Endocytic Pathway

## Graphical Abstract

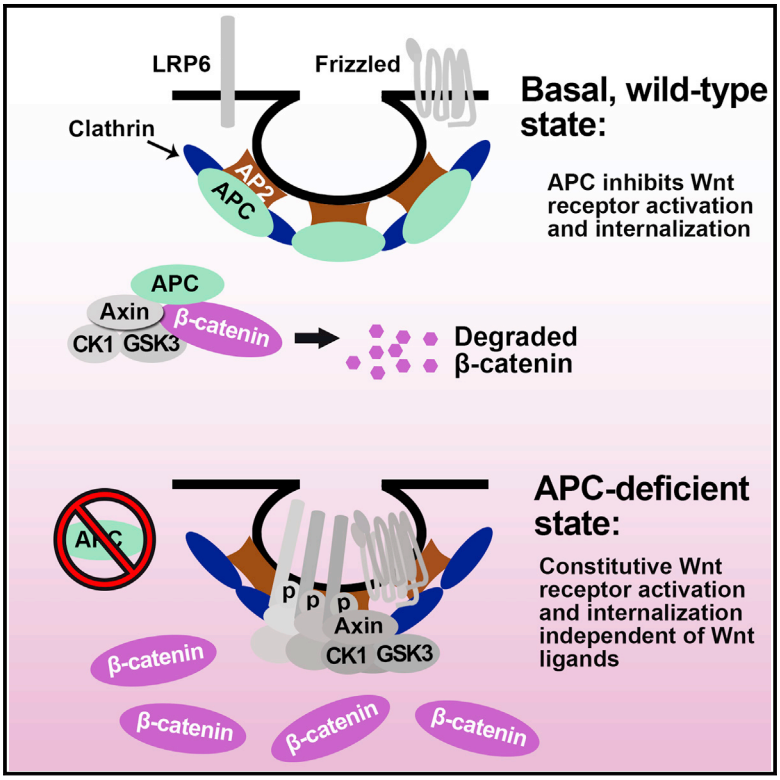


## Highlights

- APC, but not APC2, prevents ligand-independent activation of Wnt receptors
- Wnt signaling in APC-deficient cells requires Wnt pathway membrane components
- Wnt signaling in APC-deficient cells is dependent on the clathrin endocytic pathway
- APC interacts with the AP2-clathrin complex

## Authors

Kenyi Saito-Diaz, Hassina Benchabane, Ajit Tiwari, ..., David J. Robbins, Yashi Ahmed, Ethan Lee

## Correspondence

yashi.ahmed@dartmouth.edu (Y.A.), ethan.lee@vanderbilt.edu (E.L.)

## In Brief

In the absence of Wnt ligand, APC (as part of the destruction complex) maintains low cytoplasmic β-catenin. Saito-Diaz et al. show that APC regulates not only β-catenin proteolysis, but also Wnt receptor activation. APC prevents constitutive activation of Wnt receptors in mammalian cells and *Drosophila*. APC loss results in ligand-independent pathway activation via clathrin-mediated endocytosis.

Saito-Diaz et al., 2018, Developmental Cell *44*, 566–581
March 12, 2018 
https://doi.org/10.1016/j.devcel.2018.02.013

CellPress

CellPress

Developmental Cell
Article

# APC Inhibits Ligand-Independent Wnt Signaling by the Clathrin Endocytic Pathway

Kenyi Saito-Diaz,[1] Hassina Benchabane,[2] Ajit Tiwari,[3] Ai Tian,[2] Bin Li,[4] Joshua J. Thompson,[5] Annastasia S. Hyde,[1] Leah M. Sawyer,[1] Jeanne N. Jodoin,[1,6] Eduardo Santos,[1] Laura A. Lee,[7] Robert J. Coffey,[1,5] R. Daniel Beauchamp,[1,8] Christopher S. Williams,[5,9] Anne K. Kenworthy,[1,3] David J. Robbins,[4] Yashi Ahmed,[2,*] and Ethan Lee[1,9,10,*]

[1]Department of Cell & Developmental Biology, Vanderbilt University, Nashville, TN 37232, USA
[2]Department of Molecular and Systems Biology and the Norris Cotton Cancer Center, Geisel School of Medicine at Dartmouth College, Hanover, NH 03755, USA
[3]Department of Molecular Physiology and Biophysics, Vanderbilt University, Nashville, TN 37232, USA
[4]Molecular Oncology Program, Division of Surgical Oncology, Dewitt Daughtry Family Department of Surgery, and Sylvester Comprehensive Cancer Center, Miller School of Medicine, University of Miami, Miami, FL 33136, USA
[5]Department of Medicine, Vanderbilt University Medical Center, Nashville, TN 37232, USA
[6]Department of Biology, Massachusetts Institute of Technology, Cambridge, MA 02142, USA
[7]Department of Pathology, Microbiology, and Immunology, Vanderbilt University Medical Center, Nashville, TN 37232, USA
[8]Department of Surgery, Vanderbilt University Medical Center, Nashville, TN 37232, USA
[9]Vanderbilt Ingram Cancer Center, Vanderbilt University Medical Center, Nashville, TN 37232, USA
[10]Lead Contact
*Correspondence: yashi.ahmed@dartmouth.edu (Y.A.), ethan.lee@vanderbilt.edu (E.L.)
https://doi.org/10.1016/j.devcel.2018.02.013

## SUMMARY

**_Adenomatous polyposis coli_ (_APC_) mutations cause Wnt pathway activation in human cancers. Current models for APC action emphasize its role in promoting β-catenin degradation downstream of Wnt receptors. Unexpectedly, we find that blocking Wnt receptor activity in APC-deficient cells inhibits Wnt signaling independently of Wnt ligand. We also show that inducible loss of APC is rapidly followed by Wnt receptor activation and increased β-catenin levels. In contrast, APC2 loss does not promote receptor activation. We show that APC exists in a complex with clathrin and that Wnt pathway activation in APC-deficient cells requires clathrin-mediated endocytosis. Finally, we demonstrate conservation of this mechanism in _Drosophila_ intestinal stem cells. We propose a model in which APC and APC2 function to promote β-catenin degradation, and APC also acts as a molecular "gatekeeper" to block receptor activation via the clathrin pathway.**

## INTRODUCTION

In the absence of Wnt ligand, cytoplasmic β-catenin is maintained at low levels by its association with a destruction complex consisting of the scaffold proteins Axin and adenomatous polyposis coli (APC), a tumor suppressor, as well as casein kinase 1α (CK1α) and glycogen synthase kinase (GSK3). Within this complex, β-catenin is phosphorylated and targeted for degradation by the ubiquitin-proteasome system (Saito-Diaz et al., 2012). Wnt ligand binding promotes formation of a trimeric complex of Wnt and its co-receptors, Frizzled (Fz) and low-density lipoprotein receptor 5/6 (LRP5/6) (Tamai et al., 2000). Although LRP5 and LRP6 are highly similar, LRP6 is more potent in mammalian cells and *Xenopus* embryos and plays a more prominent role during vertebrate development (Saito-Diaz et al., 2012). The formation of aggregated receptors ("signalosome") promotes Axin recruitment in a process mediated by Dishevelled (Dvl) (Bilić et al., 2007; Zeng et al., 2008). Consequently, β-catenin degradation is inhibited, its cytoplasmic levels rise, and it is translocated to the nucleus where it associates with TCF transcription factors to initiate a Wnt transcriptional program (Saito-Diaz et al., 2012).

In the classical model, the role of APC is limited to β-catenin proteolysis. Herein, we report that APC also plays an essential role in inhibition of Wnt receptor activation in the unstimulated state. We identify a constitutive, clathrin-mediated pathway that activates Wnt signaling independent of Wnt ligands upon APC inactivation. These studies provide a new model for the mechanism by which the Wnt pathway is aberrantly activated upon APC loss and offer critical insight for developing novel therapeutics targeting Wnt-driven cancers.

## RESULTS

### LRP6 Is Required for Wnt Pathway Activation in *APC* Mutant Cells, but Not in Cells with Mutant β-Catenin

Loss of APC has been proposed to induce formation of a Wnt autocrine loop in colorectal cancer (CRC) (Voloshanenko et al., 2013). To test this model, we knocked down LRP6 in CRC lines, SW480 and DLD1, which contain APC mutations, and HCT116, which expresses non-degradable β-catenin (see Table S1 for information on Wnt pathway mutational status of cell lines). We found that LRP6 knockdown inhibited the Wnt reporter TOPflash (STF) and decreased cytoplasmic β-catenin levels only in SW480 and DLD1 cells (Figures 1A and S1A). To confirm that constitutive Wnt pathway activation resulting from APC loss requires LRP6, we knocked down APC and LRP6 in HEK293 cells stably

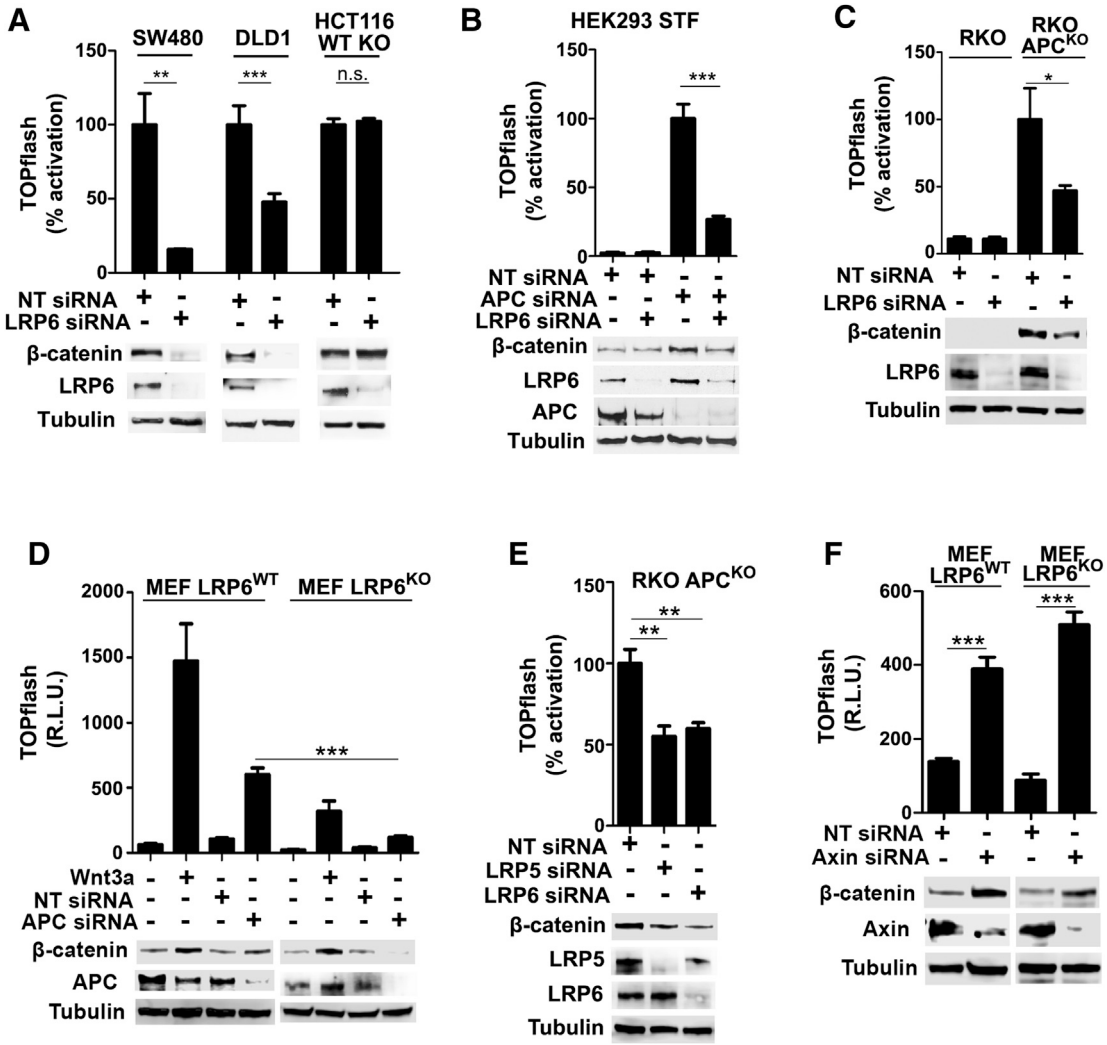


**Figure 1. LRP6 Is Required for Wnt Signaling in APC-Deficient Cells**

(A) LRP6 knockdown inhibits Wnt signaling in APC mutant CRC cells. WT KO (wild-type knockout) refers to deletion of the wild-type copy of CTNNB1.

(B–D) LRP6 knockdown prevents Wnt activation upon APC loss. HEK293 STF and (C) RKO APC$^{KO}$ cells were transfected with LRP6 small interfering RNA (siRNA) and APC siRNA. (D) MEF LRP6$^{WT}$ and MEF LRP6$^{KO}$ cells were incubated with Wnt3a or APC siRNA. R.L.U., relative light units.

(E) LRP5 and LRP6 are required for Wnt activation in the absence of APC. RKO APC$^{KO}$ cells were incubated with LRP5 or LRP6 siRNA.

(F) LRP6 is not required for Wnt activation in the absence of Axin. MEF LRP6$^{WT}$ and MEF LRP6$^{KO}$ cells were incubated with Axin siRNA.

Graph shows mean ± SEM. n.s., non-significant; *p < 0.05; **p < 0.01; ***p < 0.001. See also Figure S1.

expressing TOPflash (HEK293 STF). Activation of both TOPflash and endogenous Wnt target genes due to APC knockdown was reversed by concomitant LRP6 knockdown in HEK293 STF but not in a reporter line (HEK293-CMV) controlled by a non-Wnt-regulated promoter (Thorne et al., 2010) (Figures 1B and S1B–S1D). A similar result was observed upon APC knockdown in the RKO CRC line (Figure S1E). To rule out residual APC effects, we generated a cell line (RKO APC$^{KO}$) null for APC (Figure S1F). RKO APC$^{KO}$ cells exhibited elevated cytoplasmic β-catenin (Figure S1F), which was downregulated by LRP6 knockdown (Figure 1C). To rule out incomplete LRP6 knockdown, we tested LRP6-null mouse embryonic fibroblasts (MEF LRP6$^{KO}$) (Figure S1G). Incubation of MEF LRP6$^{KO}$ with Wnt3a resulted in decreased Wnt signaling compared with parental cells (MEF$^{WT}$). Similarly, APC knockdown stimulated Wnt signaling in MEF$^{WT}$ cells but not MEF LRP6$^{KO}$ cells (Figure 1D). These findings indicate that effects of APC loss on Wnt pathway activation are mediated partly through LRP6.

Given LRP5/6 redundancy, we speculated that low levels of Wnt signaling in MEF LRP6$^{KO}$ cells reflect LRP5 presence. Thus, we asked whether LRP5 similarly promotes Wnt activation upon APC knockdown. We found that LRP5 knockdown in RKO APC$^{KO}$ cells also inhibited Wnt activation (Figures 1E and S1H), suggesting that both co-receptors mediate Wnt activation in APC-depleted cells. We next asked whether Wnt pathway activation due to loss of another destruction complex protein, Axin, is also LRP6 dependent. In contrast to APC-depleted cells, Axin knockdown resulted in comparable Wnt pathway activation

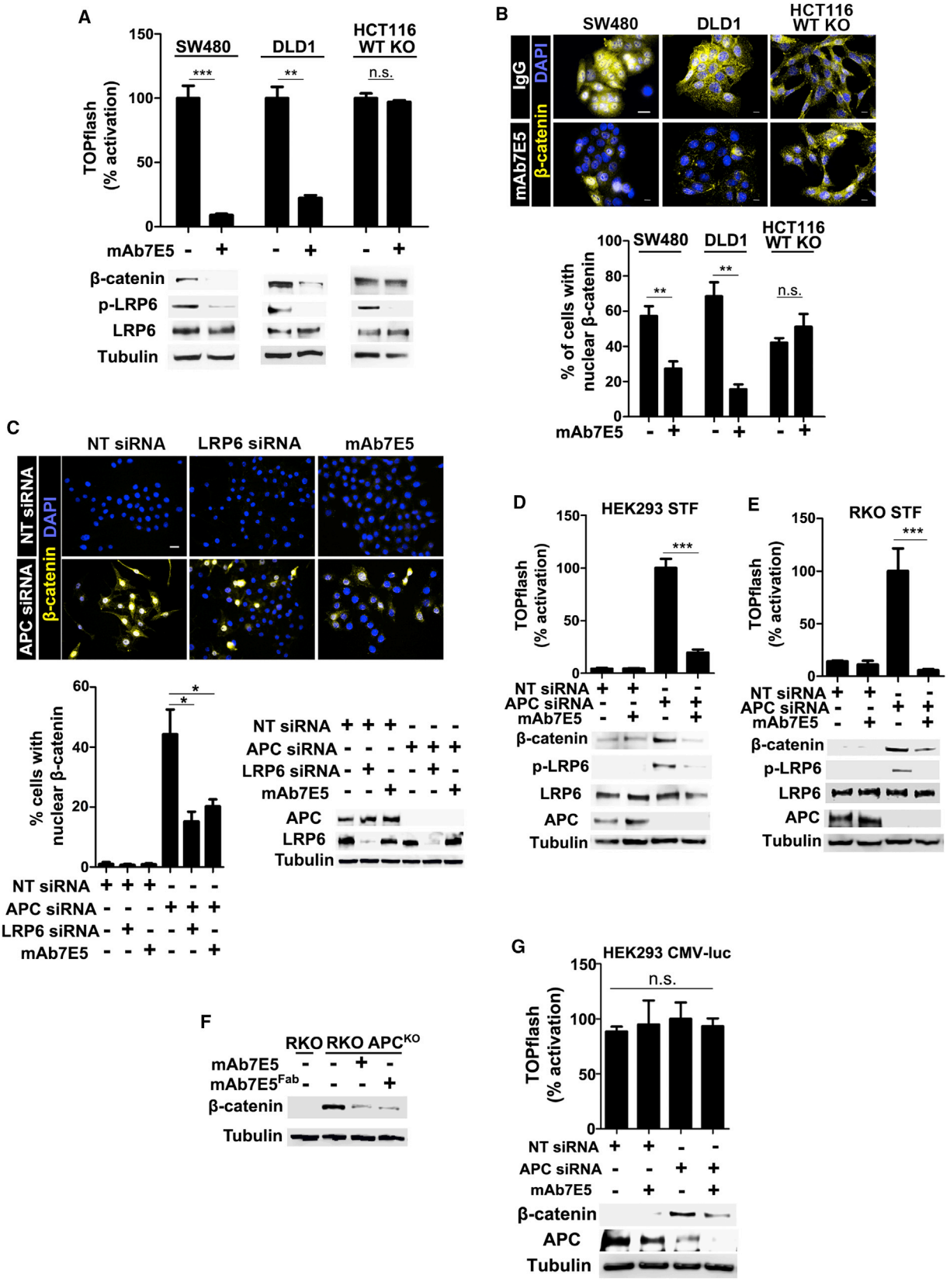


*(legend on next page)*

in MEF LRP6$^{WT}$ and MEF LRP6$^{KO}$ cells (Figures 1F and S1I). These results suggest that the requirement for LRP6 to promote Wnt signaling in APC-depleted cells is not simply due to destruction complex disruption.

### mAb7E5 Inhibits Constitutive Wnt Signaling in APC-Deficient Cells by Binding LRP6

To more acutely disrupt LRP6 function and to rule out compensatory effects of LRP6 knockdown in APC-deficient cells, we developed a monoclonal antibody (mAb7E5) against a central region of the LRP6 extracellular domain (Figure S2A). mAb7E5 blocked Wnt3a signaling in cultured cells, as indicated by TOPflash inhibition, decreased cytoplasmic β-catenin levels, and inhibition of LRP6 phosphorylation (indicative of receptor activation) (MacDonald et al., 2008) (Figures S2B–S2D). mAb7E5 inhibited Wnt activation by both Wnt1 and Wnt3a, which bind to distinct regions of the LRP6 extracellular domain (Ettenberg et al., 2010) (Figure S2E). To confirm that mAb7E5 inhibited Wnt signaling by binding LRP6, cells were transfected with full-length LRP6 (LRP6 FL) or constitutively activated LRP6 lacking the extracellular domain (LRP6ΔN) (Liu et al., 2003). mAb7E5 inhibited pathway activation by LRP6 FL but not LRP6ΔN (Figure S2F). Inhibition by mAb7E5 of Wnt signaling due to LRP6 FL overexpression suggests that the antibody may stabilize an LRP6 inactive state. As predicted, mAb7E5 did not block Wnt signaling upon treatment of cells with lithium, which inhibits GSK3 (Figure S2G). The multivalent nature of mAb7E5 is not required for its activity because its Fab fragment also inhibited Wnt signaling (Figure S2H).

We next tested whether mAb7E5 downregulates Wnt signaling in CRC cells. mAb7E5 inhibited Wnt signaling in SW480 and DLD1 but not HCT116 cells (Figures 2A and 2B). We found that all CRC cells tested exhibit elevated phospho-LRP6 levels that were decreased by mAb7E5 treatment, suggestive of autocrine feedback in these cells (Figure 2A). To confirm these results, we knocked down APC in HEK293 STF and RKO STF cells and demonstrated increased Wnt reporter activity, β-catenin accumulation, and phospho-LRP6 levels (Figures 2C–2E). mAb7E5 treatment blocked all of the effects of APC depletion (Figures 2C–2E). Similarly, mAb7E5 treatment downregulated cytoplasmic β-catenin in RKO APC$^{KO}$ cells (Figure 2F). As control, mAb7E5 had no effect on HEK293-CMV cells (Figure 2G). Together, these findings provide further evidence that the Wnt activation resulting from APC depletion depends on LRP6.

### Surface Receptor Activation, but Not Wnt Ligands, Is Required for Pathway Activation in APC Mutant Cells

We hypothesized that, like LRP6, other components of the signalosome are required for constitutive Wnt pathway activation upon APC loss. Thus, inhibiting other membrane components (e.g., Fz or Dvl) should inhibit Wnt signaling in *APC* mutant cells. To simultaneously block multiple Fz and Dvl isoforms, we expressed their dominant-negative forms, Fz1-ER or Xdd1, respectively (Kaykas et al., 2004; Wallingford et al., 2000) (Figure 3A). Fz1-ER or Xdd1 expression inhibited Wnt reporter activity and reduced phospho-LRP6 in APC-depleted cells (Figure 3B). Consistent with the latter, APC knockdown cells null for all three *Dvl* genes (Dvl TKO) (Gammons et al., 2016) failed to activate Wnt signaling, in contrast to treatment of Dvl TKO cells with GSK3 inhibitors, CHIR-99021 (CHIR) or lithium (Figures 3C and 3D). As control, inhibiting Fz or Dvl did not suppress Wnt signaling induced by lithium (Figure 3E).

These findings suggested that multiple signalosome components mediate the aberrantly increased signaling resulting from APC loss. We therefore tested whether loss of APC induced signalosome formation. The receptor aggregates or signalosomes that form upon Wnt ligand activation are detectable as multiprotein complexes in sucrose density gradients (Bilić et al., 2007). As expected, we observed a shift in the migration of LRP6 into the denser fractions of lysates from RKO cells treated with Wnt3a compared with untreated cells (Figure 3F). However, LRP6 was also detected in the denser fractions of lysates from RKO APC$^{KO}$ cells even in the absence of Wnt3a, suggesting aggregate formation (Figure 3F). Based on these findings, we conclude that APC loss induces signalosome assembly.

We next tested whether Wnt ligands were necessary for the aberrant signaling in *APC* mutant cells. A chimeric protein encoding the immunoglobulin Fc domain fused to the cysteine-rich region of Fz8 (Fz8-Fc) sequesters Wnt ligands to block Wnt pathway activation (DeAlmeida et al., 2007). Fz8-Fc inhibited Wnt reporter activity and β-catenin accumulation in Wnt3a-treated cells (Figure 4A). Fz8-Fc, however, had no effect on Wnt reporter activity in APC-deficient cells (Figures 4B–4D). Similarly, secreted Frizzled-related protein 1 (sFRP-1) sequesters Wnt ligands to block ligand-dependent Wnt signaling (Saito-Diaz et al., 2012). sFRP-1 inhibited Wnt signaling in Wnt3a-treated cells but not *APC*-null cells (Figures S3A and S3B). In contrast, we found that the secreted factor, Dkk1, which binds LRP5/6 (Semënov et al., 2001), inhibited Wnt signaling in APC-deficient cells (Figure S3C). APC-deficient cells remained responsive to exogenous Wnt3a activation, as indicated by increased phospho-LRP6, which was inhibited by Fz8-Fc (Figure 4E). The lack of increased Wnt reporter activity and β-catenin levels likely reflects maximal pathway stimulation in RKO APC$^{KO}$ cells. We conclude that Wnt ligands are dispensable for pathway activation resulting from APC loss.

To further rule out a requirement for Wnt ligands, we inhibited their secretion. Wnt ligand palmitoylation by Porcupine

**Figure 2. mAb7E5 Inhibits Wnt Signaling upon APC Loss**

(A) mAb7E5 inhibits Wnt signaling in *APC* mutant CRC cells. CRC cells were incubated with mAb7E5 followed by immunoblotting.

(B and C) mAb7E5 prevents accumulation of nuclear β-catenin. (B) CRC cells incubated with mAb7E5 or (C) RKO cells treated with APC siRNA and either LRP6 siRNA or mAb7E5 were immunostained. Scale bar, 40 μm.

(D and E) mAb7E5 inhibits Wnt signaling upon APC loss. (D) HEK293 STF and (E) RKO STF cells were incubated with APC siRNA and mAb7E5.

(F) mAb7E5 blocks Wnt pathway activation in APC-deficient cells. RKO APC$^{KO}$ cells were incubated with mAb7E5 or mAb7E5$^{Fab}$ followed by immunoblotting.

(G) Specificity of Wnt signaling inhibition by mAb7E5 in APC-deficient cells. A non-Wnt-regulated reporter cell line, HEK293 CMV-luc, was incubated with APC siRNA and mAb7E5.

Graph shows mean ± SEM. n.s., non-significant; *$p < 0.05$; **$p < 0.01$; ***$p < 0.001$. See also Figure S2.

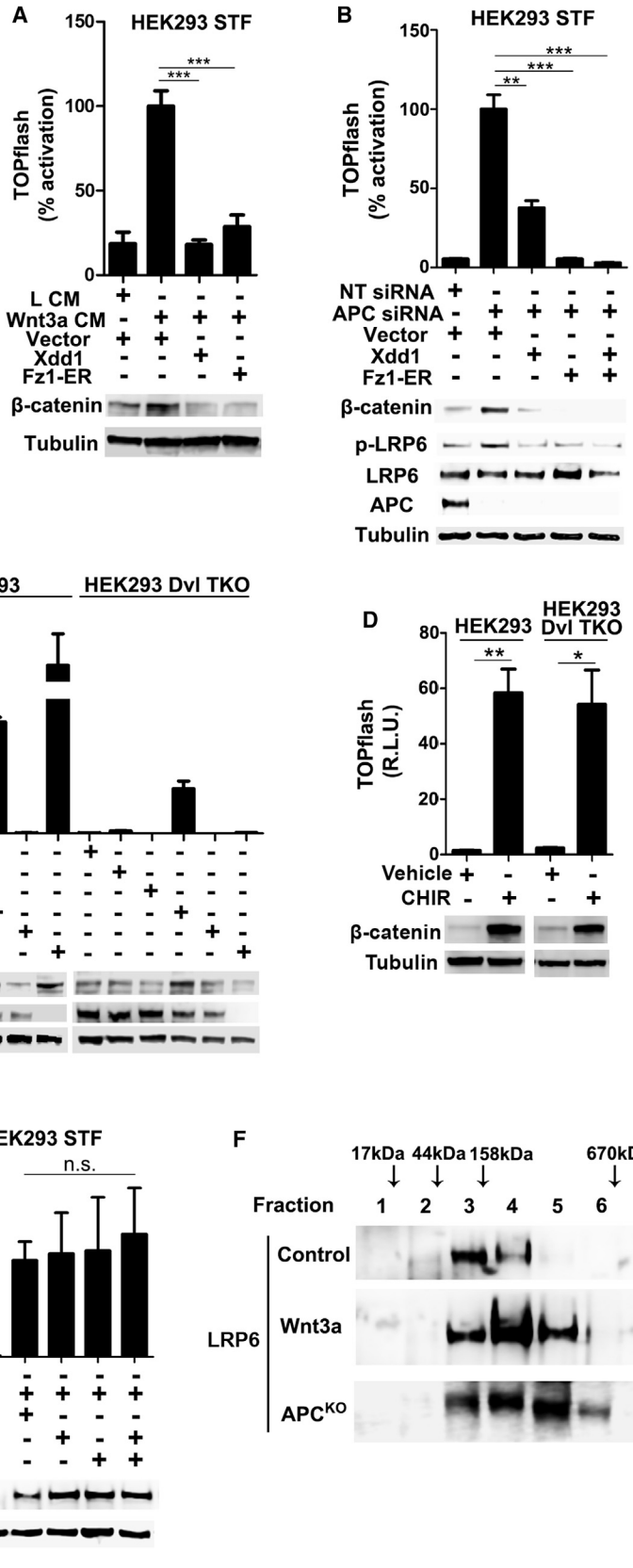


*(legend on next page)*

(PORCN), an O-acyltransferase, is required for secretion and receptor binding (Saito-Diaz et al., 2012; Janda et al., 2012). As expected, two PORCN inhibitors, Wnt-C59 ($IC_{50}$ [half maximal inhibitory concentration] = 0.1nM) and IWP-2 ($IC_{50}$ = 27nM) (Chen et al., 2009; Proffitt et al., 2013), inhibited Wnt signaling in Wnt3a-transfected cells (Figures 4F and S3D) but not when Wnt3a was added exogenously (Figures 4G and S3E). Wnt-C59 and IWP-2 also had no observable effect on Wnt signaling in APC-deficient cells (Figures 4H–4J and S3F–S3H). In contrast with APC mutant CRC cells, we observed decreased phospho-LRP6 in HCT116 cells upon Fz8-Fc, Wnt-C59, or IWP-2 treatment, suggesting that an autocrine feedback circuit occurs in HCT116 cells; reporter activity, however, was not inhibited (Figures 4D, 4J, and S3H).

To rule out residual PORCN activity, we knocked down APC in *PORCN* null cells, which are non-responsive to transfected Wnt3a (Barrott et al., 2011) (Figure S3I). In contrast with Dvl TKO cells, APC knockdown in *PORCN* null cells activated Wnt signaling, which was inhibited by LRP6 knockdown (Figure 4K). These results further support a model in which APC loss leads to ligand-independent activation of Wnt receptors and downstream signaling.

## Rapid Accumulation of Phospho-LRP6 and β-Catenin Stabilization Occur Immediately upon Loss of APC

We asked if receptor activation upon APC loss was a secondary consequence of a simple positive-feedback mechanism resulting from Wnt target gene regulation. We found that lithium treatment stabilized β-catenin and promoted Wnt reporter activity, but, in contrast to APC, did not promote phospho-LRP6 accumulation (Figure 5A). We also tested the effects of a dominant-negative TCF4 (dnTCF4) (van de Wetering et al., 2002) that prevents TCF-mediated expression of Wnt target genes. We found that dnTCF4 inhibited reporter activation, but not accumulation of β-catenin or phospho-LRP6, upon APC knockdown (Figures 5B and 5C). Thus, stabilization of β-catenin and activation of Wnt target genes are not sufficient to activate Wnt receptors upon APC loss.

APC has multiple activities in addition to its Wnt signaling role (Saito-Diaz et al., 2012). Aberrant Wnt activation in *APC* mutant cells is rescued by an APC fragment ($APC^T$) containing its β-catenin and Axin binding domains (Li et al., 2012) (Figure 5D). We found that $APC^T$ suppresses Wnt signaling and LRP6 phosphorylation in APC-deficient cells (Figures 5E–5G), suggesting that LRP6 activation in APC mutant cells is due to loss of the APC region required for its Wnt pathway function.

If formation of an active Wnt receptor complex were not due to a transcriptional/translational feedback mechanism in APC-deficient cells, LRP6 phosphorylation and β-catenin stabilization upon APC loss should be temporally correlated. To test this hypothesis, we assessed the timing of LRP6 phosphorylation and β-catenin accumulation after APC loss. We fused $APC^T$ to an auxin-inducible degron (AID) that mediates auxin-induced turnover (Holland et al., 2012) by the plant E3 TIR1 protein (Figure 5D). Transfection of AID-Myc-mCherry-$APC^T$ into RKO $APC^{KO}$ cells stably expressing E3 TIR1 suppressed Wnt signaling to a similar extent as $APC^T$ (Figure 5H). Auxin addition resulted in rapid loss of AID-Myc-mCherry-$APC^T$ (within 30 min) that paralleled β-catenin stabilization. Furthermore, β-catenin accumulation paralleled phospho-LRP6 appearance (Figure 5H). To rule out a role for protein secretion in Wnt pathway activation upon APC loss, cells were preincubated with Brefeldin A (BFA), which blocks transport from the endoplasmic reticulum to the Golgi (Misumi et al., 1986). We found that BFA did not affect LRP6 phosphorylation or β-catenin accumulation upon loss of AID-Myc-mCherry-$APC^T$ (Figure 5I). Although unlikely, we cannot rule out the possibility that an unknown factor in preformed secretory vesicles is immediately released upon loss of AID-Myc-mCherry-$APC^T$.

Finally, we asked why, if APC is essential for the destruction complex, β-catenin is still degraded in APC-depleted cells upon receptor disruption. APC and APC2 are structurally similar (Figure 5D). We found that APC2 knockdown increased β-catenin levels but not receptor activation. Thus, although both APC and APC2 promote β-catenin degradation, only APC regulates receptor activation (Figures 5J and 5K). This result explains why blocking receptor activation in APC-deficient cells allows for subsequent β-catenin turnover: APC2 can compensate for loss of APC in the destruction complex. Consistent with this model, we found that APC2 knockdown in *APC*-null cells blocked the effects of mAb7E5 on β-catenin degradation in RKO $APC^{KO}$ cells (Figure 5L).

## Endocytosis Is Required for Wnt Signaling upon APC Loss

Endocytosis is required for receptor-mediated activation of the Wnt pathway (Blitzer and Nusse, 2006; Gagliardi et al., 2014; Yamamoto et al., 2006). Endocytosis is highly sensitive to low temperature, which has been used extensively to study this process (Silverstein et al., 1977). We found that inhibiting endocytosis by shifting Wnt3a-treated RKO or RKO $APC^{KO}$ cells to 4°C decreased cytoplasmic β-catenin and phospho-LRP6 levels; this effect was reversed by shifting cells back to 37°C. In contrast, activating RKO cells with lithium or CHIR had no effect on cytoplasmic β-catenin levels at 4°C (Figures 6A–6D and

**Figure 3. Loss of APC Promotes Ligand-Independent Signalosome Formation**

(A) Fz and Dvl are required for ligand-mediated Wnt activation. HEK293 STF cells were transfected with Xdd1 and Fz1-ER for 24 hr and then incubated with L-cell conditioned medium (L CM) or Wnt3a conditioned medium (Wnt3a CM).

(B) Dvl and Fz are required for Wnt activation in APC-deficient cells. HEK293 STF cells were transfected with APC siRNA plus Xdd1 or Fz1-ER.

(C) APC depletion fails to activate the Wnt pathway in *Dvl* null cells. HEK293 and HEK293 Dvl TKO were transfected with APC siRNA or treated with Wnt3a CM or 30 mM LiCl.

(D) GSK3 inhibition activates the Wnt pathway in Dvl null cells. HEK293 Dvl TKO cells were incubated with 2 μM CHIR.

(E) Wnt signaling due to β-catenin stabilization is not dependent on Fz or Dvl. HEK293 STF cells were transfected with Xdd1 or Fz1-ER and incubated with 30 mM LiCl.

(F) Similar to Wnt ligand-activated cells, LRP6 forms high molecular complexes in the absence of APC (sucrose density gradient analysis).

Graphs show mean ± SEM. n.s., non-significant; *p < 0.05; **p < 0.01; ***p < 0.001.

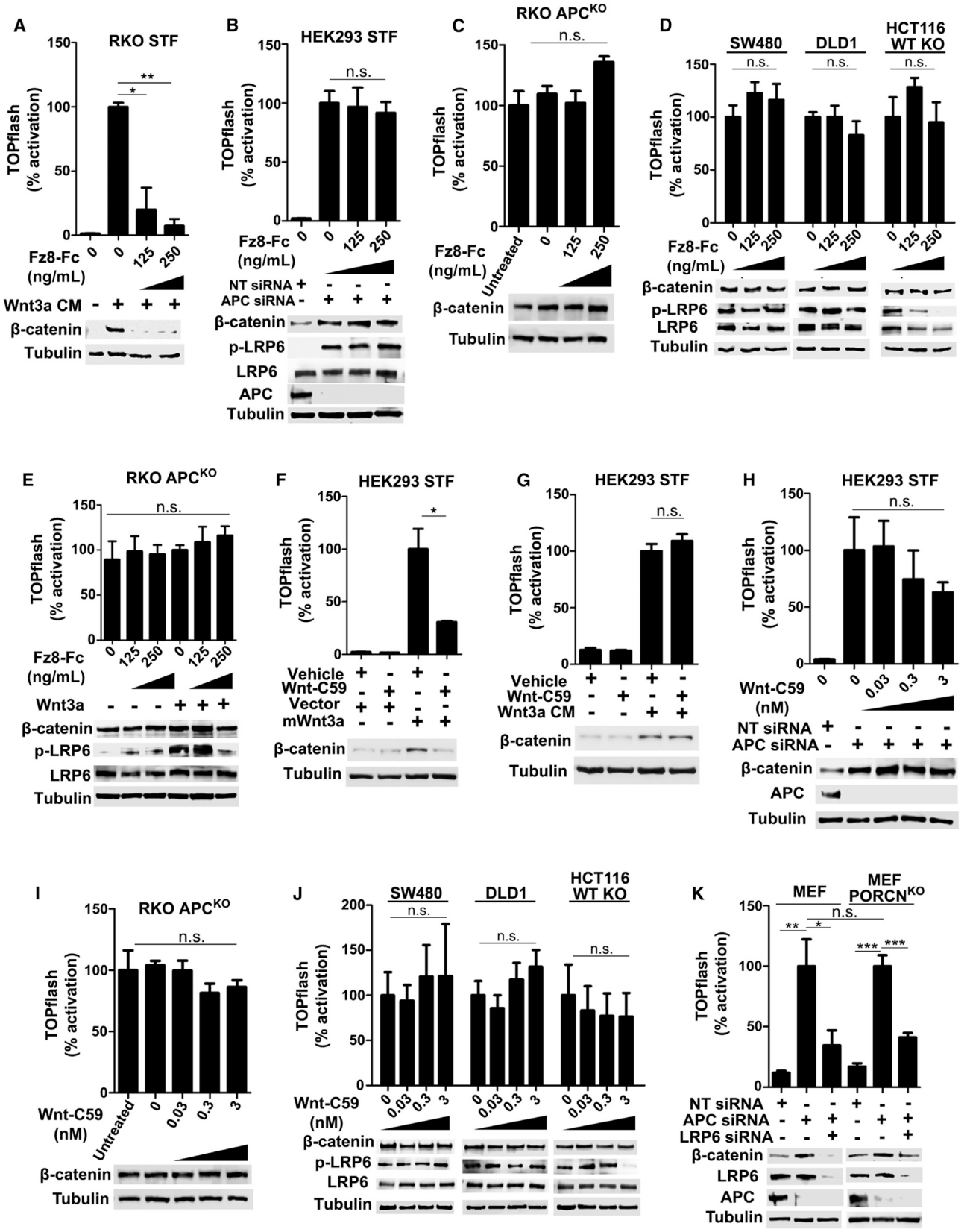


*(legend on next page)*

S4A–S4D). Similarly, we found that shifting APC-depleted retinal pigmented epithelium (RPE) cells or SW480 (APC mutant), but not HCT116 (β-catenin mutant) cells, to 4°C decreased cytoplasmic β-catenin (Figures S4E and S4F). To further test the requirement for endocytosis, we used a dominant-negative Dynamin (Dynamin$^{K44A}$), which inhibits both clathrin- and caveolin-mediated endocytosis as well as Wnt signaling (Blitzer and Nusse, 2006; Dutta and Donaldson, 2012; Yamamoto et al., 2008). Dynamin$^{K44A}$ decreased β-catenin levels in all APC-deficient cell lines tested (Figures 6E, S4G, and S4H).

Given that Dynamin is required for Wnt pathway activation in APC-deficient cells, we asked whether LRP6 is internalized upon APC loss. Consistent with previous reports (Yamamoto et al., 2006), we found that LRP6 was internalized within 2 hr after Wnt3a addition and could be blocked by mAb7E5 (Figure 6F and Movie S1). As expected, lithium had no effect on LRP6 internalization (Figure 6F). LRP6 internalization upon APC knockdown was blocked by mAb7E5 but not by PORCN inhibitors (Figures 6G and S4I). In RPE cells, fluorescence intensity profiles from an axial scan showed two distinct peaks of LRP6-eYFP signal that corresponded with high concentrations of LRP6 at the plasma membrane. In contrast, in APC-depleted cells, we observed multiple peaks corresponding with large, punctate, LRP6-containing structures postulated to represent intracellular vesicles (Bilić et al., 2007). Treatment of APC-depleted cells with mAb7E5 re-established formation of two predominant peaks of fluorescence signal (Figures 6G and S4J). These studies provide further evidence that the endocytic pathway is required for Wnt activation in APC-deficient cells.

## Wnt Receptor Activation in APC-Deficient Cells Occurs via a Clathrin-Dependent Mechanism

Clathrin- and caveolin-mediated endocytosis have both been implicated in Wnt signaling (Bilić et al., 2007; Blitzer and Nusse, 2006; Yamamoto et al., 2006). Pitstop-2 and nystatin are small-molecule inhibitors of clathrin- and caveolin-mediated endocytosis, respectively (Dutta and Donaldson, 2012; Yamamoto et al., 2006). Consistent with a previous study (Yamamoto et al., 2006), nystatin, but not Pitstop-2, inhibited Wnt3a-mediated β-catenin accumulation in RKO cells (Figures 7A and S5A). In RKO APC$^{KO}$ cells, however, Pitstop-2 decreased β-catenin, whereas nystatin had no effect (Figures 7B and S5B). Similar results were observed for chloroquine, another inhibitor of clathrin-mediated endocytosis (Dutta and Donaldson, 2012) (Figure S5C). To confirm these results, we showed that knockdown of caveolin, but not clathrin, inhibited Wnt3a signaling in RKO cells (Figures 7C, S5D, and S5E). In contrast, knockdown of clathrin, but not caveolin, inhibited Wnt signaling in RKO APC$^{KO}$ cells (Figure 7D). We next assessed whether inhibition of clathrin- or caveolin-mediated endocytosis altered LRP6-eYFP localization in APC-deficient cells. Pitstop-2 promoted LRP6-eYFP accumulation at the plasma membrane, whereas nystatin treatment had no effect (Figure S5F). These studies provide further evidence that Wnt signaling in APC-depleted cells occurs via a clathrin-mediated mechanism.

A previous study showed that disruption of clathrin-mediated endocytosis in mouse fibroblast L cells inhibits Wnt ligand-mediated activation (Blitzer and Nusse, 2006). We found that Wnt3a signaling in L cells is mediated by both clathrin- and caveolin-dependent pathways (Figure S5G). Wnt pathway activation upon APC knockdown, however, is dependent on clathrin in both L cells (Figure S5G) and a MEF cell line deficient for caveolin (Hanson et al., 2013) (Figure S5H). Thus, the requirement for caveolin versus clathrin for Wnt ligand activation appears to be cell-type dependent, whereas clathrin is specifically required for constitutive Wnt pathway activation in APC-deficient cells, regardless of cell type.

We next tested whether APC influences clathrin- or caveolin-mediated endocytosis via their physical interaction. Immunofluorescence studies revealed significant overlap of APC with clathrin, but not caveolin, at the plasma membrane in RPE cells (Figures 7E–7G). To corroborate these findings, we performed co-immunoprecipitation studies and found that endogenous APC was pulled down with clathrin and its adaptor protein, AP-2, but not with caveolin (Figure 7H). We found that APC$^{T}$ similarly co-immunoprecipitated with endogenous clathrin, suggesting that APC$^{T}$, which contains the Axin and β-catenin binding domains of APC, is sufficient for interaction with the clathrin complex (Figure S5I).

## Wnt Receptor Activation and Clathrin-Dependent Internalization Promotes Wnt Signaling in APC$^{min}$ Organoids

Organoid cultures represent a powerful *ex vivo* system to model development and disease. We tested whether LRP6 and clathrin-mediated endocytosis are required for maintenance of organoids derived from intestinal adenomas of *APC$^{min}$* mice that normally do not require exogenous Wnt ligands for growth and maintenance (Sato et al., 2011). Pitstop-2 inhibited *APC$^{min}$* organoid growth and reduced cytoplasmic β-catenin; these

**Figure 4. Wnt Receptor Activation in APC-Deficient Cells Is Wnt Ligand Independent**

(A–D) Fz8-Fc blocks Wnt ligand-mediated signaling but not signaling in APC-deficient cells. (A) RKO STF cells were incubated with Wnt3a and Fz8-Fc at the indicated concentrations. (B) HEK293 STF cells transfected with APC siRNA and (C) RKO APC$^{KO}$ cells were incubated with Fz8-Fc. (D) Wnt activation in CRC cells is not dependent on Wnt ligand. CRC cells were incubated for 48 hr with Fz8-Fc at the indicated concentrations.

(E) APC-depleted cells are responsive to Wnt ligand. RKO APC$^{KO}$ cells were preincubated for 30 min with Fz8-Fc followed by incubation with Wnt3a.

(F) Inhibition of secreted Wnt3a by the PORCN inhibitor Wnt-C59. HEK293 STF were transfected with Wnt3a and treated with Wnt-C59 (0.3 nM).

(G) Wnt pathway activation by exogenous Wnt3a is not blocked by Wnt-C59. HEK293 STF cells were preincubated for 30 min with Wnt-C59 followed by incubation with Wnt3a.

(H and I) PORCN inhibition does not block Wnt activation upon loss of APC. (H) HEK293 STF cells transfected with APC siRNA and (I) RKO APC$^{KO}$ cells were incubated with Wnt-C59.

(J) PORCN inhibition does not block Wnt activation in CRC cells. CRC cells were incubated for 48 hr with Wnt-C59.

(K) LRP6 is required for Wnt activation upon loss of APC in the absence of PORCN. PORCN$^{KO}$ MEF and wild-type MEF were transfected with APC and LRP6 siRNA.

Graphs show mean ± SEM. n.s., non-significant; *$p < 0.05$; **$p < 0.01$; ***$p < 0.001$. See also Figure S3.

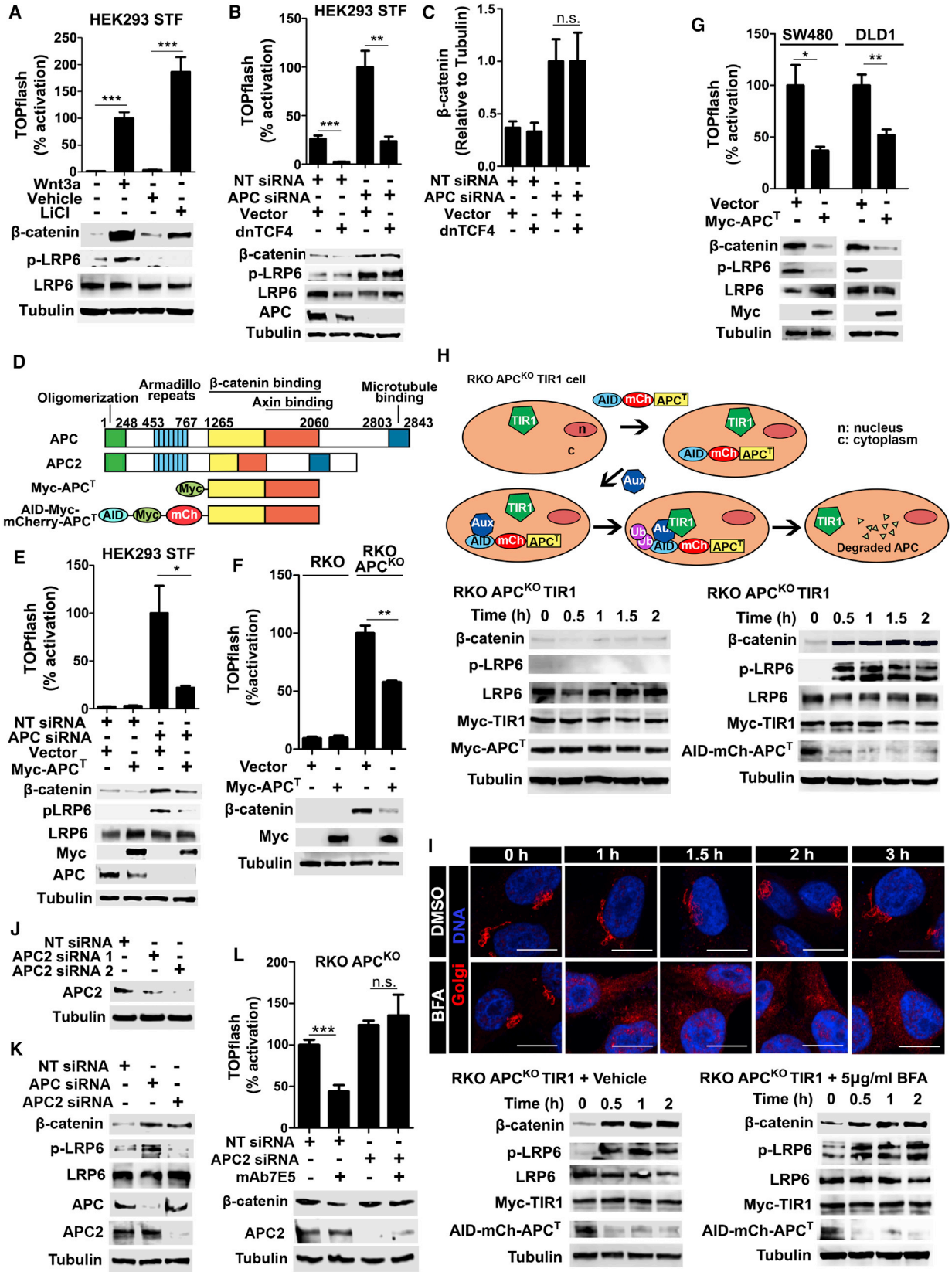


(legend on next page)

effects were reversed by Wnt3a addition (Figures S6A and S6B). Addition of mAb7E5 reduced cytoplasmic β-catenin levels and promoted formation of multiple protrusions reminiscent of crypt-like structures seen in wild-type enteroids (Figures S6C and S6D). Differences in growth inhibition between Pitstop-2- and mAb7E5-treated $APC^{min}$ organoids may reflect greater Wnt inhibition by Pitstop-2 due to its higher cell permeability. Consistent with this possibility, we found that LRP6 knockdown by small hairpin RNA (shRNA) lentivirus treatment inhibited growth of $APC^{min}$ organoids (Figures S6E and S6D).

### *Drosophila* Arrow/LRP6 and Dsh/Dvl Are Required for the Aberrant Activation of Wingless Signaling in the *Apc1* Mutant Intestine

We sought to determine whether the constitutive activation of Wnt signaling resulting from APC loss requires Wnt receptor activation *in vivo*. Consistent with our findings in cultured cells, previous epistasis analysis in *Drosophila* suggested that the *Dvl* homolog (*dishevelled*; *dsh*) acts genetically downstream of *Apc2* in the embryonic epidermis (McCartney et al., 1999). To test this conclusion in a distinct physiological context, we examined the *Drosophila* midgut. Similar to the effects of *APC* inactivation in the mammalian adult intestine (Saito-Diaz et al., 2012; Sansom et al., 2004), loss of *Apc1* in the *Drosophila* adult midgut results in aberrant transcriptional regulation of Wg target genes, overproliferation of intestinal stem cells (ISCs), and disruption of epithelial cell polarity (Cordero et al., 2012; Tian et al., 2016, 2017). We first tested whether ISC overproliferation and disrupted cell polarity resulting from *Apc1* inactivation are dependent on either the *Drosophila* LRP6 homolog (Arrow; Arr) or Dsh (Klingensmith et al., 1994; Noordermeer et al., 1994; Wehrli et al., 2000). A significantly increased number of progenitor cells (ISCs and enteroblasts), marked by their expression of *esg>GFP* (*esg-gal4*, *UAS-GFP*) (Micchelli and Perrimon, 2006), was observed in the posterior midgut of 1- to 2-day-old *Apc1* null adults compared with controls (Figures 8A, 8B, 8E, 8F, and 8Q). In contrast, RNAi-mediated knockdown of either *arr* or *dsh* in intestinal progenitor cells during adult midgut development resulted in a significant reduction of progenitor cell number in *Apc1* nulls (Figures 8I, 8J, 8M, 8N, and 8Q). Furthermore, the disrupted epithelial cell polarity in *Apc1* nulls (Tian et al., 2017), as indicated by aberrant subcellular localization of an adherens junction component, Armadillo (Arm), was also rescued by Arrow depletion (Figures 8C, 8D, 8G, 8H, 8K, and 8L). To rule out RNAi off-target effects, we tested two independently derived *arr* knockdown lines and obtained similar results (Figure 8Q).

To confirm these findings with an independent approach, we examined the effects of RNAi-mediated knockdown of *Apc1* either singly or with concomitant knockdown of *arr* or *dsh*, *Apc1*, *arr*, or *dsh* were knocked down during adult midgut formation using the temperature-sensitive progenitor cell driver $esg^{ts}$. Consistent with the *Apc1* null mutant phenotype, knockdown of *Apc1* specifically in progenitor cells resulted in an increase in their number in the posterior midgut of 1- to 2-day-old adults (Figures S7A–S7D and S7H–S7K). In contrast, concomitant RNAi-mediated knockdown of *Apc1* and either *dsh* or *arr* resulted in significant reduction of progenitor cell number compared with knockdown of *Apc1* alone (Figures S7E–S7G and S7L–S7N). To rule out RNAi off-target effects, we tested multiple independently derived *arr* and *dsh* knockdown lines and observed similar effects (Figures S7G and S7N). Therefore, in the *Drosophila* midgut, both Arrow and Dsh are required to mediate the aberrant activation of Wg signaling resulting from Apc1 loss.

We next tested whether this requirement for Arrow and Dsh is independent of Wg ligand from progenitor cells. We found that RNAi-mediated knockdown in progenitors of either *wg* or *wntless* (*wls*), which encodes a transmembrane protein essential for Wg secretion (Bänziger et al., 2006; Bartscherer et al., 2006), had no significant effect on increased progenitor cell number and did not rescue the disrupted epithelial cell polarity in *Apc1* mutant midguts (Figure 8R). These findings provide *in vivo* evidence that Wg secretion from progenitor cells is not required for the phenotypic consequences of Apc1 loss, although a possible role for Wg from other intestinal cell types remains unknown.

Finally, to determine whether the constitutive activation of Wg target gene expression in *Apc1* mutants requires signalosome components, we examined a transcriptional reporter for *naked cuticle* (*nkd*), a direct target gene of Armadillo/β-catenin-TCF (Zeng et al., 2000). Wg and its target genes are expressed at high levels at all the boundaries between major compartments in the adult intestine (Buchon et al., 2013; Tian et al., 2016); as such, *nkd-lacZ* is expressed in a gradient that peaks at the midgut-hindgut compartment boundary and extends into the posterior midgut (Tian et al., 2016) (Figure S8A). In *Apc1* mutants, aberrant activation of Wg signaling resulted in ectopic expression of *nkd-lacZ* in the posterior midgut (Figures S8B and S8F). Importantly, RNAi-mediated knockdown of either *arr* or *dsh* in

**Figure 5. LRP6 Activation and β-Catenin Accumulation Occur Rapidly upon Loss of APC**

(A) Degradation complex inhibition does not lead to LRP6 phosphorylation. HEK293 STF cells were incubated with Wnt3a or 30 mM LiCl.

(B and C) Inhibition of Wnt-mediated transcription does not block LRP6 activation. (B) HEK293 STF cells were transfected with APC siRNA and dnTCF4. β-catenin levels were quantified and the average of five independent replicates are plotted in (C).

(D) Schematics of APC structure and truncations tested.

(E–G) β-catenin and Axin binding domains of APC are sufficient to rescue loss-of-APC phenotype. (E) HEK293 STF treated with APC siRNA, (F) RKO $APC^{KO}$, and (G) CRC cells were transfected with Myc-$APC^{T}$ followed by TOPflash analysis and immunoblotting.

(H and I) Loss of APC correlates with β-catenin and phospho-LRP6 accumulation independently of secreted ligands. (H) RKO $APC^{KO}$ TIR1 cells were transfected with Myc-$APC^{T}$ or AID-Myc-mCherry-$APC^{T}$ followed by incubation with auxin. (I) RKO $APC^{KO}$ TIR1 cells were transfected with AID-Myc-mCherry-$APC^{T}$ followed by incubation with BFA and auxin. AID, auxin-inducible degron; mCh, mCherry; Aux, auxin. Scale bar, 10 μm.

(J) Downregulation of APC2 by two distinct siRNAs.

(K) Loss of APC2 promotes Wnt pathway but not receptor activation. HEK293 cells were incubated with APC or APC2 siRNA.

(L) APC2 is required for β-catenin degradation complex in APC-null cells. RKO $APC^{KO}$ cells were incubated with APC2 siRNA and mAb7E5.

Graphs show mean ± SEM. n.s., non-significant; *$p < 0.05$; **$p < 0.01$; ***$p < 0.001$.

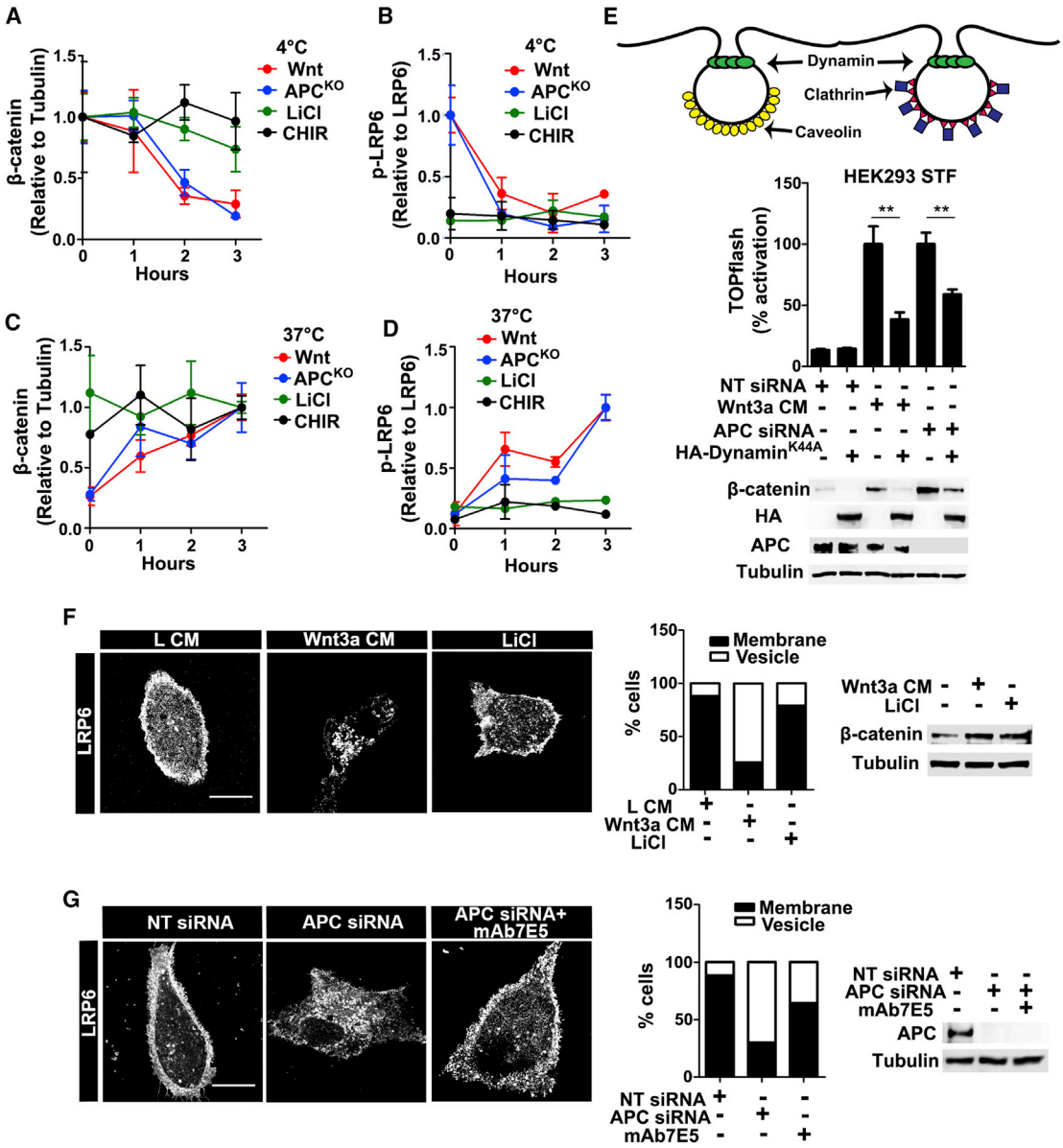


**Figure 6. Endocytosis Is Required for Wnt Signaling in APC-Deficient Cells**

(A–D) Inhibition of endocytosis induced by temperature shift prevents β-catenin accumulation and LRP6 phosphorylation. RKO cells (treated with Wnt3a, 30 mM LiCl, or 2 μM CHIR), and RKO APC$^{KO}$ cells were incubated at 4°C (A and B) and shifted back to 37°C (C and D). The average of three independent replicates were plotted. Representative blots are shown in Figures S4A–S4D.

(E) Dynamin is required for Wnt signaling in APC-depleted cells. HEK293 STF cells were incubated with Wnt3a or APC siRNA and transfected with HA-Dynamin$^{K44A}$. Graphs show mean ± SEM. n.s., non-significant; **$p < 0.01$.

(F and G) LRP6 is internalized in Wnt3a-treated and APC-deficient cells. RPE cells were transfected with LRP6-eYFP and incubated with (F) Wnt3a or 30 mM LiCl or (G) APC siRNA and mAb7E5. Cells (>100 per condition) demonstrating membrane or internalized LRP6 were quantified. Scale bars, 20 μm.

See also Figure S4.

*Apc1* mutants significantly reduced ectopic *nkd-lacZ* expression (Figures S8D–S8F), whereas RNAi-mediated knockdown of the control gene *yellow* (*y*) had no effect (Figures S8C and S8F). Together, these findings provide *in vivo* evidence that both Arr and Dsh are required for ectopic expression of Wg target genes in *Apc1* mutants and that the requirement for Wnt pathway signalosome components in mediating the consequences of APC loss is evolutionarily conserved.

## DISCUSSION

Despite extensive investigation, the mechanistic basis for APC function in Wnt signaling has remained an enigma (Saito-Diaz et al., 2012). Based on our results, we propose that a major role of APC is to prevent constitutive, ligand-independent, clathrin-dependent signalosome formation and Wnt pathway activation (Figure S8G). Consistent with this model, the secreted

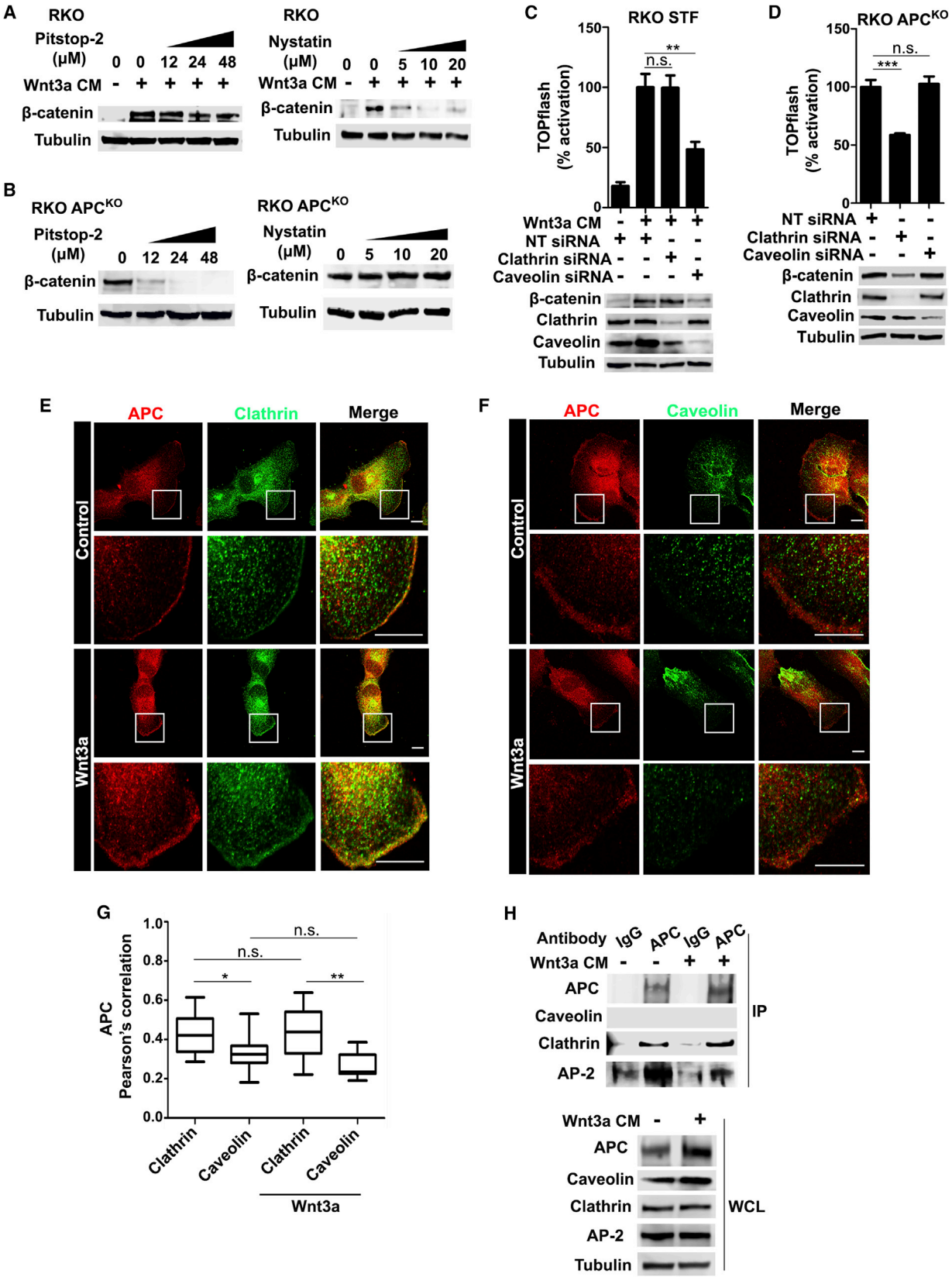


(legend on next page)

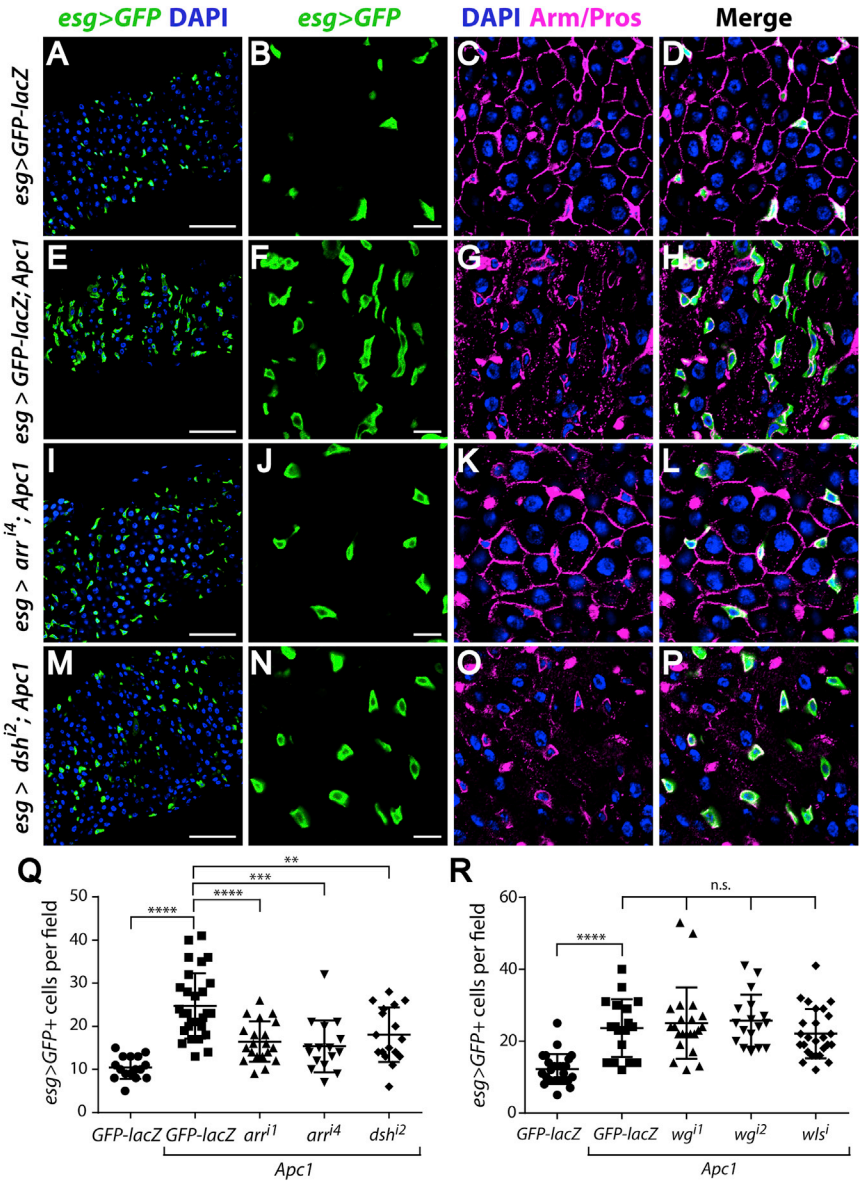


**Figure 8. Arrow and Dishevelled Are Required for the Consequences of *Apc1* Loss in *Drosophila* ISCs Independently of Wnt Ligand**

(A–H and Q) In comparison with controls (A–D and Q), *Apc1* mutation leads to increased progenitor cell number (E, F, H, and Q) and cell polarity defects (G). Intestinal progenitor cells are marked with *esg>GFP* (green), cell membranes with Armadillo/β-catenin (Arm, magenta), nuclei with DAPI (blue), and enteroendocrine cells with Prospero (Pros, magenta).

(I–L and Q) RNAi-mediated Arrow knockdown in *Apc1* mutants leads to significant reduction of progenitor cell number (I, J, L, and Q) and rescue of cell polarity defects (K).

(M–P and Q) RNAi-mediated Dsh knockdown in *Apc1* mutants leads to significant reduction of progenitor cell number (M, N, P, and Q).

(A, E, I, and M) Lower magnification view (scale bars, 50 μm). (B–D, F–H, J–L, and N–P) Higher magnification view (scale bar, 10 μm).

(R) RNAi-mediated knockdown of Wg or Wls in *Apc1* mutants does not reduce progenitor cell number.

Graphs show mean ± SD. **p < 0.01, ***p < 0.001, ****p < 0.0001.

inhibitors, Fz8-Fc and sFRP-1, which bind and sequester Wnt ligands, are not capable of inhibiting Wnt signaling in APC mutant cells. This is in contrast to DKK1, which either binds directly to LRP6 to inhibit signaling via disruption of the LRP-Fz complex or promotes internalization of inactive LRP6 receptor (Yamamoto et al., 2008).

It is possible that signaling upon APC loss is due to the presence of certain Wnt ligands that are resistant to the actions of Fz8-Fc and sFRP-1 and that do not require PORCN or Wntless for secretion. It is even possible that the released ligand may not be a member of the Wnt family. However, based on our Auxin-APC studies, such a ligand must already be present in secretory vesicles and released upon APC loss of function; we consider this possibility unlikely. Furthermore, our *in vivo* findings in the *Drosophila* intestine support the conclusion that Wingless and Wntless are not required for the activation of Wnt signaling resulting from APC loss. These results are consistent with a previous genetic epistasis study in the *Drosophila* embryo, in which the authors concluded that *wg* acts upstream of *Apc2* and thus is not required to activate signaling in *Apc2* mutants (McCartney et al., 1999). However, the authors noted that the phenotype of the *wg; Apc2* double mutant is less severe than the *Apc2* single mutant, making interpretation of the epistasis challenging. Thus, it remains possible that the epistasis relationship may differ in

**Figure 7. Clathrin-Mediated Endocytosis Is Required for Wnt Signaling in APC-Deficient Cells**

(A–D) Ligand-dependent and -independent Wnt activation requires distinct endocytic pathways. (A) RKO cells incubated with Wnt3a or (B) RKO APC$^{KO}$ cells were incubated with the indicated concentrations of Pitstop-2 or nystatin. (C) RKO cells incubated with Wnt3a were transfected with caveolin-1 or clathrin siRNA. (D) RKO APC$^{KO}$ cells were transfected with clathrin or caveolin-1 siRNA.

(E–G) APC partially colocalizes with clathrin but not caveolin-1. (E and F) RPE cells were incubated with or without Wnt3a, fixed, and stained for APC and clathrin or caveolin. Scale bar, 10 μm. (G) Intensity correlation analysis of APC-clathrin/caveolin-1 signal.

(H) APC co-immunoprecipitates with clathrin and its adaptor protein, AP2.

Graphs show mean ± SEM. n.s., non-significant; **p < 0.01; ***p < 0.001. See also Figure S5.

the embryonic epidermis versus the adult gut epithelium, reflecting potential context-specificity in the activation of signaling following Apc loss.

Our findings are consistent with the proposed role of APC and APC2 in β-catenin phosphorylation and degradation (Saito-Diaz et al., 2012). Thus, in the absence of APC, APC2 could act as the primary scaffold protein in the β-catenin degradation complex to promote β-catenin turnover. Such redundancy could explain why β-catenin can still be degraded in certain cells (e.g., intestinal epithelium) upon APC loss when the Wnt receptor complex is disrupted (Figure S8G). Consistent with an expanded role in Wnt signaling for APC compared with APC2, phenotypes associated with APC2 inactivation are often not as severe as those due to APC loss. For example, APC inactivation results in early embryonic lethality in mice, whereas *APC2* null mutants are viable and display neuronal defects that disrupt learning and memory reminiscent of Sotos syndrome (Almuriekhi et al., 2015). In addition, APC2 knockout in the brain results in neuronal defects but does not stabilize β-catenin (Shintani et al., 2012). These reports are consistent with our findings showing that, although APC2 can compensate for loss of the destruction complex activity of APC, APC2 is not capable of compensating for APC in regulating the Wnt receptor complex. In some contexts (e.g., mammalian epithelium), APC and APC2 are functionally redundant (Daly et al., 2016). It is possible that, in these tissues, another mechanism may inhibit Wnt receptor activation upon APC loss. This may also explain why *APC* mutations predominate in a select number of human cancers.

Previous studies provide evidence for both caveolin- and clathrin-based mechanisms in Wnt pathway activation (Bilić et al., 2007; Blitzer and Nusse, 2006; Yamamoto et al., 2006); the predominant mechanism may be dependent on cell type (Feng and Gao, 2015; Kim et al., 2013). Consistent with this idea, we found that epithelial cells (e.g., HEK293, RKO, and RPE cells) mediate Wnt signaling via the caveolin pathway, whereas fibroblasts (e.g., L cells and MEFs) mediate Wnt signaling via the clathrin pathway. The clathrin-mediated pathway can be promiscuous: a well-known example is the constitutive internalization of the transferrin receptor. Thus, it is possible that APC acts as a "gatekeeper" for receptor activation via the clathrin endocytic pathway in the absence of Wnt ligand. Notably, our proposed model does not preclude Wnt pathway activation via the caveolin pathway. Thus, *APC* mutant cells may retain the capacity to respond to Wnt ligands. Future studies will focus on the detailed mechanism by which APC regulates this process.

## STAR★METHODS

Detailed methods are provided in the online version of this paper and include the following:

- KEY RESOURCES TABLE
- CONTACT FOR REAGENT AND RESOURCE SHARING
- EXPERIMENTAL MODEL AND SUBJECT DETAILS
  - Cell Lines
  - Three-Dimensional Organoid Culture
  - Drosophila Stocks
- METHOD DETAILS
  - Transfections
  - Immunoblots and Immunoprecipitation
  - Generation of the mAb7E5 Antibody
  - Generation of RKO APC$^{KO}$
  - Generation of Stable Cell Lines
  - Sucrose Density Gradients
  - Endocytosis Assays
  - Microscopy
  - Live Cell Imaging
  - Organoid Lentiviral Transduction
  - Organoid Immunofluorescence
  - Drosophila RNAi Experiments
  - Drosophila Immunohistochemistry
  - Auxin-Dependent Degradation Assay
  - Reporter Assay
  - RNA Isolation and qRT-PCR
- QUANTIFICATION AND STATISTICAL ANALYSIS
  - Immunoblotting Quantification
  - Line Scan Analysis
  - Organoid Measurement
  - Statistical Analysis
  - Colocalization Analysis

### SUPPLEMENTAL INFORMATION

Supplemental Information includes eight figures, two tables, and one movie and can be found with this article online at https://doi.org/10.1016/j.devcel.2018.02.013.

### ACKNOWLEDGMENTS

We thank Bloomington *Drosophila* Stock Center and Vienna *Drosophila* Research Center for *Drosophila* lines, the Vanderbilt Antibody and Protein Resource, and the Nikon Center of Excellence at Vanderbilt University. We thank Dr. Abel Alcazar-Roman for critical reading of this manuscript. This work was funded by NIH grants (R01CA105038, R01GM122222, and R01121421 to Y.A.; NCIP5095103 Special Programs of Research Excellence in GI Cancer to R.J.C.; T32GM007347 and F30DK111107 to J.J.T.; R01DK099204 to C.S.W; CA069457, GI SPORE P50CA095103, and VICC P30CA068485 to R.D.B.; R01GM106720 to A.K.K.; R01GM081635, R01GM103926, and R35GM122516 to E.L.; P40OD018537 to the BDSC), the Norris Cotton Cancer Center (to Y.A.), a VA MERIT 2I01BX001426 (to C.S.W.), and two CTSA awards (UL1TR000445 and UL1TR002243) from the National Center for Advancing Translational Sciences (to E.L.).

### AUTHOR CONTRIBUTIONS

K.S.-D. conceived of, designed, executed, and interpreted the experiments. H.B., A. Tian, and Y.A. designed and performed the *Drosophila* experiments. B.L. performed PCR-based and *APC$^{min}$* organoids studies. L.M.S. and J.N.J. performed microscopy-based studies. J.J.T. performed the LRP6 shRNA knockdown of *APC$^{min}$* organoids. A.S.H. developed the RKO APC$^{KO}$ cell line and provided intellectual input. E.S. performed biochemical experiments. A. Tiwari performed co-localization microscopy-based studies. L.A.L. provided intellectual input and manuscript editing. A.K.K., D.J.R., C.S.W., R.J.C., and R.D.B. provided reagents and intellectual input. E.L. provided intellectual guidance and reagents. K.S.-D., H.B., Y.A., and E.L. wrote the manuscript.

### DECLARATION OF INTERESTS

E.L. and D.J.R. are co-founders of StemSynergy Therapeutics, a company that seeks to develop inhibitors of major signaling pathways (including the Wnt pathway) for the treatment of cancer.

Received: March 16, 2017
Revised: January 2, 2018
Accepted: February 13, 2018
Published: March 12, 2018

## REFERENCES

Ahmed, D., Eide, P.W., Eilertsen, I.A., Danielsen, S.A., Eknæs, M., Hektoen, M., Lind, G.E., and Lothe, R.A. (2013). Epigenetic and genetic features of 24 colon cancer cell lines. Oncogenesis *2*, e71.

Ahmed, Y., Hayashi, S., Levine, A., and Wieschaus, E. (1998). Regulation of Armadillo by a *Drosophila* APC inhibits neuronal apoptosis during retinal development. Cell *93*, 1171–1182.

Almuriekhi, M., Shintani, T., Fahiminiya, S., Fujikawa, A., Kuboyama, K., Takeuchi, Y., Nawaz, Z., Nadaf, J., Kamel, H., Kitam, A.K., et al. (2015). Loss-of-function mutation in APC2 causes Sotos syndrome features. Cell Rep. *10*, 1585–1598.

Bänziger, C., Soldini, D., Schütt, C., Zipperlen, P., Hausmann, G., and Basler, K. (2006). Wntless, a conserved membrane protein dedicated to the secretion of Wnt proteins from signaling cells. Cell *125*, 509–522.

Barrott, J.J., Cash, G.M., Smith, A.P., Barrow, J.R., and Murtaugh, L.C. (2011). Deletion of mouse Porcn blocks Wnt ligand secretion and reveals an ectodermal etiology of human focal dermal hypoplasia/Goltz syndrome. Proc. Natl. Acad. Sci. USA *108*, 12752–12757.

Bartscherer, K., Pelte, N., Ingelfinger, D., and Boutros, M. (2006). Secretion of Wnt ligands requires Evi, a conserved transmembrane protein. Cell *125*, 523–533.

Bilić, J., Huang, Y.-L., Davidson, G., Zimmermann, T., Cruciat, C.-M., Bienz, M., and Niehrs, C. (2007). Wnt induces LRP6 signalosomes and promotes Dishevelled-dependent LRP6 phosphorylation. Science *316*, 1619–1622.

Blitzer, J.T., and Nusse, R. (2006). A critical role for endocytosis in Wnt signaling. BMC Cell Biol. *7*, 28.

Buchon, N., Osman, D., David, F.P., Fang, H.Y., Boquete, J.P., Deplancke, B., and Lemaitre, B. (2013). Morphological and molecular characterization of adult midgut compartmentalization in *Drosophila*. Cell Rep. *3*, 1725–1738.

Chen, B., Dodge, M.E., Tang, W., Lu, J., Ma, Z., Fan, C.W., Wei, S., Hao, W., Kilgore, J., Williams, N.S., et al. (2009). Small molecule-mediated disruption of Wnt-dependent signaling in tissue regeneration and cancer. Nat. Chem. Biol. *5*, 100–107.

Cordero, J.B., Stefanatos, R.K., Myant, K., Vidal, M., and Sansom, O.J. (2012). Non-autonomous crosstalk between the Jak/Stat and Egfr pathways mediates Apc1-driven intestinal stem cell hyperplasia in the *Drosophila* adult midgut. Development *139*, 4524–4535.

Daly, C.S., Shaw, P., Ordonez, L.D., Williams, G.T., Quist, J., Grigoriadis, A., Van Es, J.H., Clevers, H., Clarke, A.R., and Reed, K.R. (2016). Functional redundancy between Apc and Apc2 regulates tissue homeostasis and prevents tumorigenesis in murine mammary epithelium. Oncogene *36*, 1793–1803.

DeAlmeida, V.I., Miao, L., Ernst, J.A., Koeppen, H., Polakis, P., and Rubinfeld, B. (2007). The soluble Wnt receptor Frizzled8CRD-hFc inhibits the growth of teratocarcinomas in vivo. Cancer Res. *67*, 5371–5379.

Dutta, D., and Donaldson, J.G. (2012). Search for inhibitors of endocytosis. Cell. Logist. *2*, 203–208.

Ettenberg, S.A., Charlat, O., Daley, M.P., Liu, S., Vincent, K.J., Stuart, D.D., Schuller, A.G., Yuan, J., Ospina, B., Green, J., et al. (2010). Inhibition of tumorigenesis driven by different Wnt proteins requires blockade of distinct ligand-binding regions by LRP6 antibodies. Proc. Natl. Acad. Sci. USA *107*, 15473–15478.

Feng, Q., and Gao, N. (2015). Keeping Wnt signalosome in check by vesicular traffic. J. Cell. Physiol. *230*, 1170–1180.

Gagliardi, M., Hernandez, A., McGough, I.J., and Vincent, J.-P. (2014). Inhibitors of endocytosis prevent Wnt/Wingless signalling by reducing the level of basal β-catenin/Armadillo. J. Cell Sci. *127*, 4918–4926.

Gammons, M.V., Rutherford, T.J., Steinhart, Z., Angers, S., and Bienz, M. (2016). Essential role of the Dishevelled DEP domain in a Wnt-dependent human-cell-based complementation assay. J. Cell Sci. *129*, 3892–3902.

Guo, Z., Driver, I., and Ohlstein, B. (2013). Injury-induced BMP signaling negatively regulates *Drosophila* midgut homeostasis. J. Cell Biol. *201*, 945–961.

Hanson, C.A., Drake, K.R., Baird, M.A., Han, B., Kraft, L.J., Davidson, M.W., and Kenworthy, A.K. (2013). Overexpression of Caveolin-1 is sufficient to phenocopy the behavior of a disease-associated mutant. Traffic *14*, 663–677.

Holland, A.J., Fachinetti, D., Han, J.S., and Cleveland, D.W. (2012). Inducible, reversible system for the rapid and complete degradation of proteins in mammalian cells. Proc. Natl. Acad. Sci. USA *109*, E3350–E3357.

Janda, C.Y., Waghray, D., Levin, A.M., Thomas, C., and Garcia, K.C. (2012). Structural basis of Wnt recognition by frizzled. Science *337*, 59–64.

Kaykas, A., Yang-Snyder, J., Héroux, M., Shah, K.V., Bouvier, M., and Moon, R.T. (2004). Mutant Frizzled 4 associated with vitreoretinopathy traps wild-type Frizzled in the endoplasmic reticulum by oligomerization. Nat. Cell Biol. *6*, 52–58.

Kim, I., Pan, W., Jones, S.A., Zhang, Y., Zhuang, X., and Wu, D. (2013). Clathrin and AP2 are required for PtdIns(4,5)P2-mediated formation of LRP6 signalosomes. J. Cell Biol. *200*, 419–428.

Klingensmith, J., Nusse, R., and Perrimon, N. (1994). The *Drosophila* segment polarity gene dishevelled encodes a novel protein required for response to the wingless signal. Genes Dev. *8*, 118–130.

Li, B., Orton, D., Neitzel, L.R., Astudillo, L., Shen, C., Long, J., Chen, X., Kirkbride, K.C., Doundoulakis, T., Guerra, M.L., et al. (2017). Differential abundance of CK1α provides selectivity for pharmacological CK1α activators to target WNT-dependent tumors. Sci. Signal. *10*, eaak9916.

Li, V.S.W., Ng, S.S., Boersema, P.J., Low, T.Y., Karthaus, W.R., Gerlach, J.P., Mohammed, S., Heck, A.J.R., Maurice, M.M., Mahmoudi, T., et al. (2012). Wnt signaling through inhibition of β-catenin degradation in an intact Axin1 complex. Cell *149*, 1245–1256.

Liu, G., Bafico, A., Harris, V.K., and Aaronson, S.A. (2003). A novel mechanism for Wnt activation of canonical signaling through the LRP6 receptor. Mol. Cell. Biol. *23*, 5825–5835.

MacDonald, B.T., Yokota, C., Tamai, K., Zeng, X., and He, X. (2008). Wnt signal amplification via activity, cooperativity, and regulation of multiple intracellular PPPSP motifs in the Wnt co-receptor LRP6. J. Biol. Chem. *283*, 16115–16123.

McCartney, B.M., Dierick, H.A., Kirkpatrick, C., Moline, M.M., Baas, A., Peifer, M., and Bejsovec, A. (1999). *Drosophila* Apc2 is a cytoskeletally-associated protein that regulates Wingless signaling in the embryonic epidermis. J. Cell Biol. *146*, 1303–1318.

Micchelli, C.A., and Perrimon, N. (2006). Evidence that stem cells reside in the adult *Drosophila* midgut epithelium. Nature *439*, 475–479.

Misumi, Y., Miki, K., Takatsuki, A., Tamura, G., and Ikehara, Y. (1986). Novel blockade by brefeldin A of intracellular transport of secretory proteins in cultured rat hepatocytes. J. Biol. Chem. *261*, 11398–11403.

Miyoshi, H., and Stappenbeck, T.S. (2013). In vitro expansion and genetic modification of gastrointestinal stem cells in spheroid culture. Nat. Protoc. *12*, 2471–2482.

Noordermeer, J., Klingensmith, J., Perrimon, N., and Nusse, R. (1994). dishevelled and armadillo act in the Wingless signalling pathway in *Drosophila*. Nature *367*, 80–83.

Proffitt, K.D., Madan, B., Ke, Z., Pendharkar, V., Ding, L., Lee, M.A., Hannoush, R.N., and Virshup, D.M. (2013). Pharmacological inhibition of the Wnt acyltransferase PORCN prevents growth of WNT-driven mammary cancer. Cancer Res. *73*, 502–507.

Rambhatla, L., Chiu, C.P., Glickman, R.D., and Rowe-Rendleman, C. (2002). In vitro differentiation capacity of telomerase immortalized human RPE cells. Invest. Ophthalmol. Vis. Sci. *43*, 1622–1630.

Saito-Diaz, K., Chen, T.W., Wang, X., Thorne, C.A., Wallace, H.A., Page-McCaw, A., and Lee, E. (2012). The way Wnt works: components and mechanism. Growth Factors *31*, 1–31.

Sansom, O.J., Reed, K.R., Hayes, A.J., Ireland, H., Brinkmann, H., Newton, I.P., Batlle, E., Simon-Assmann, P., Clevers, H., Nathke, I.S., et al. (2004).

Loss of Apc in vivo immediately perturbs Wnt signaling, differentiation, and migration. Genes Dev. *18*, 1385–1390.

Sato, T., Stange, D.E., Ferrante, M., Vries, R.G., Van Es, J.H., Van den Brink, S., Van Houdt, W.J., Pronk, A., Van Gorp, J., Siersema, P.D., et al. (2011). Long-term expansion of epithelial organoids from human colon, adenoma, adenocarcinoma, and Barrett's epithelium. Gastroenterology *141*, 1762–1772.

Semënov, M.V., Tamai, K., Brott, B.K., Kühl, M., Sokol, S., and He, X. (2001). Head inducer Dickkopf-1 is a ligand for Wnt coreceptor LRP6. Curr. Biol. *11*, 951–961.

Silverstein, S.C., Steinman, R.M., and Cohn, Z.A. (1977). Endocytosis. Annu. Rev. Biochem. *46*, 669–722.

Shintani, T., Takeuchi, Y., Fujikawa, A., and Noda, M. (2012). Directional neuronal migration is impaired in mice lacking Adenomatous Polyposis Coli 2. J. Neurosci. *32*, 6468–6484.

Tamai, K., Semenov, M., Kato, Y., Spokony, R., Liu, C., Katsuyama, Y., Hess, F., Saint-Jeannet, J.-P., and He, X. (2000). LDL-receptor-related proteins in Wnt signal transduction. Nature *407*, 530–535.

Thorne, C.A., Hanson, A.J., Schneider, J., Tahinci, E., Orton, D., Cselenyi, C.S., Jernigan, K.K., Meyers, K.C., Hang, B.I., Waterson, A.G., et al. (2010). Small-molecule inhibition of Wnt signaling through activation of casein kinase 1a. Nat. Chem. Biol. *6*, 829–836.

Tian, A., Benchabane, H., Wang, Z., and Ahmed, Y. (2016). Regulation of stem cell proliferation and cell fate specification by Wingless/Wnt signaling gradients enriched at adult intestinal compartment boundaries. PLoS Genet. *12*, e1005822.

Tian, A., Benchabane, H., Wang, Z., Zimmerman, C., Xin, N., Perochon, J., Kalna, G., Sansom, O.J., Cheng, C., Cordero, J.B., et al. (2017). Intestinal stem cell overproliferation resulting from inactivation of the APC tumor suppressor requires the transcription cofactors Earthbound and Erect wing. PLoS Genet. *13*, e1006870.

van de Wetering, M., Sancho, E., Verweij, C., de Lau, W., Oving, I., Hurlstone, A., van der Horn, K., Batlle, E., Coudreuse, D., Haramis, A.P., et al. (2002). The β-catenin/TCF-4 complex imposes a crypt progenitor phenotype on colorectal cancer cells. Cell *111*, 241–250.

Voloshanenko, O., Erdmann, G., Dubash, T.D., Augustin, I., Metzig, M., Moffa, G., Hundsrucker, C., Kerr, G., Sandmann, T., Anchang, B., et al. (2013). Wnt secretion is required to maintain high levels of Wnt activity in colon cancer cells. Nat. Commun. *4*, 2610.

Wallingford, J.B., Rowning, B.A., Vogeli, K.M., Rothbächer, U., Fraser, S.E., and Harland, R.M. (2000). Dishevelled controls cell polarity during *Xenopus* gastrulation. Nature *405*, 81–85.

Wehrli, M., Dougan, S.T., Caldwell, K., O'Keefe, L., Schwartz, S., Vaizel-Ohayon, D., Schejter, E., Tomlinson, A., and DiNardo, S. (2000). arrow encodes an LDL-receptor-related protein essential for Wingless signalling. Nature *407*, 527–530.

Willert, K., Brown, J.D., Danenberg, E., Duncan, A.W., Weissman, I.L., Reya, T., Yates, J.R., 3rd, and Nusse, R. (2003). Wnt proteins are lipid-modified and can act as stem cell growth factors. Nature *423*, 448–452.

Yamamoto, H., Komekado, H., and Kikuchi, A. (2006). Caveolin is necessary for Wnt-3a-dependent internalization of LRP6 and accumulation of beta-catenin. Dev. Cell *11*, 213–223.

Yamamoto, H., Sakane, H., Michiue, T., and Kikuchi, A. (2008). Wnt3a and Dkk1 regulate distinct internalization pathways of LRP6 to tune the activation of beta-catenin signaling. Dev. Cell *15*, 37–48.

Zeng, X., Huang, H., Tamai, K., Zhang, X., Harada, Y., Yokota, C., Almeida, K., Wang, J., Doble, B., Woodgett, J., et al. (2008). Initiation of Wnt signaling: control of Wnt coreceptor Lrp6 phosphorylation/activation via frizzled, dishevelled and axin functions. Development *135*, 367–375.

Zeng, W., Wharton, K.A., Mack, J.A., Wang, K., Gadbaw, M., Suyama, K., Klein, P.S., and Scott, M.P. (2000). naked cuticle encodes an inducible antagonist of Wnt signalling. Nature *403*, 789–795.

Zhong, Z., Baker, J.J., Zylstra-Diegel, C.R., and Williams, B.O. (2012). Lrp5 and Lrp6 play compensatory roles in mouse intestinal development. J. Cell. Biochem. *113*, 31–38.

## STAR★METHODS

### KEY RESOURCES TABLE

| REAGENT or RESOURCE | SOURCE | IDENTIFIER |
|---|---|---|
| Antibodies | | |
| Mouse anti-β-catenin | Vanderbilt Protein and Antibody Resource | N/A |
| Mouse anti-Myc (9E10) | Vanderbilt Protein and Antibody Resource | N/A |
| Mouse anti-HA (12CA5) | Vanderbilt Protein and Antibody Resource | N/A |
| Mouse anti-Tubulin (E7) | Vanderbilt Protein and Antibody Resource | RRID: AB_2315513 |
| Rabbit anti-APC | Santa Cruz | Cat# sc-7930; RRID: AB_2242804 |
| Mouse anti-APC | Santa Cruz | Cat# sc-9998; RRID: AB_626664 |
| Rabbit anti-LRP5 (D80F2) | Cell Signaling | Cat# 5731; RRID: AB_10705602 |
| Rabbit anti-LRP6 (C5C7) | Cell Signaling | Cat# 2560; RRID: AB_10831525 |
| Rabbit anti-LRP6 (C47E12) | Cell Signaling | Cat# 3395; RRID: AB_1950408 |
| Rabbit anti-Caveolin-1 | BD Biosciences | Cat# 610060; RRID: AB_397472 |
| Mouse anti-Caveolin-1 | BD Biosciences | Cat# 610406; RRID: AB_397788 |
| Rabbit anti-Clahtrin HC | Cell Signaling | Cat# 4796; RRID: AB_10828486 |
| Mouse anti-Clahtrin HC | BD Biosciences | Cat# 610499; RRID: AB_397865 |
| Rabbit anti-p-LRP6 | EMD Millipore | Cat# 07-2187; RRID: AB_10807023 |
| Rabbit anti-Giantin | Abcam | Ca# ab24586; RRID: AB_448163 |
| Goat anti-Axin | R&D Systems | Cat# AF3287; RRID: AB_2062418 |
| Rabbit anti-APC2 | Abcam | Cat# ab80018; RRID: AB_2040524 |
| Rabbit anti-GAPDH | Cell Signaling | Cat# 5174; RRID: AB_10622025 |
| Mouse anti-B-gal | Promega | RRID: AB_2314509 |
| Mouse anti-Armadillo | Developmental Studies Hybridoma Bank | RRID: AB_528089 |
| Mouse anti-Prospero | Developmental Studies Hybridoma Bank | RRID: AB_528440 |
| Chicken anti-GFP | Abcam | Cat# ab13970; RRID: AB_300798 |
| Control Rabbit IgG | Santa Cruz | Cat# sc-2027; RRID: AB_737197 |
| Control Mouse IgG | Santa Cruz | Cat# sc-2025; RRID: AB_737182 |
| Control Human IgG | ThermoFisher | Cat# 31154; RRID: AB_243591 |
| Anti-mouse IgG HRP | Promega | Cat# W4021; RRID: AB_430834 |
| Anti-rabbit IgG HRP | Promega | Cat# W4011; RRID: AB_430833 |
| Anti-mouse Alexa Fluor 488 | ThermoFisher | Cat# A-21202; RRID: AB_141607 |
| Anti-mouse Alexa Fluor 555 | ThermoFisher | Cat# A28180; RRID: AB_2536164 |
| Anti-mouse Alexa Fluor 546 | ThermoFisher | Cat# A10036; RRID: AB_2534012 |
| Anti-rabbit Alexa Fluor 488 | ThermoFisher | Cat# A-11008; RRID: AB_143165 |
| Anti-chicken Alexa Fluor 488 | ThermoFisher | Cat# A-11039; RRID: AB_142924 |
| Anti-mouse Cy3 | Jackson Immuno | Cat#115-165-146; RRID: AB_2338690 |
| Hoechst 33342 | ThermoFisher | Cat# H1399 |
| DRAQ5 | ThemoFisher | Cat# 62251 |
| Bacterial and Virus Strains | | |
| BL21(DE3) | ThermoFisher | Cat# C600003 |
| Chemicals, Peptides, and Recombinant Proteins | | |
| IWP-2 | StemRD | Cat# 50-176-017 |
| Wnt-C59 | Cellagen Technologies | Cat# C7641-2s |
| Chloroquine diphosphate | Sigma | Cat# C6628 |
| Nystatin | EMD Millipore | Cat# 475921 |
| CHIR99021 | TOCRIS Bioscience | Cat# 4423 |
| Pitstop-2 | Abcam | Cat# ab120687 |

(*Continued on next page*)

*Continued*

| REAGENT or RESOURCE | SOURCE | IDENTIFIER |
|---|---|---|
| Fz8-Fc | R&D Systems | Cat# 6129-FZ-050 |
| Wnt3a | Time Bioscience | Cat# rmW3aH |
| Brefeldin A | Sigma | Cat# B7651 |
| sFRP-1 | R&D Systems | Cat# 9019-SF-025 |
| 1-Naphthaleneacetic acid | Sigma | Cat# N0640 |
| Critical Commercial Assays | | |
| Protein Precipitation Kit | National Diagnostics | Cat# EC-888 |
| Steady Glo Luciferase Assay System | Promega | Cat# E2510 |
| Dual Glo Luciferase Assay System | Promega | Cat# E2920 |
| CellTiter-Glo Luminiscent Cell Viability Assay | Promega | Cat# G7570 |
| High-Capacity cDNA Reverse Transcription Kit | ThermoFisher | Cat# 4368814 |
| Experimental Models: Cell Lines | | |
| HEK293 | ATCC | CRL-1573 |
| HEK293 STF | Laboratory of Jeremy Nathans. Thorne et al., 2010 | N/A |
| RKO | ATCC | CRL-2577 |
| RKO APCKO | This paper | N/A |
| RKO STF | This paper | N/A |
| RPE | Laboratory of Irina Kaverina | N/A |
| RPE shAPC | This paper | N/A |
| SW480 STF | Thorne et al., 2010 | N/A |
| DLD1 | ATCC | CCL-221 |
| DLD1 STF | This paper | N/A |
| HCT116 WTKO | Laboratory of Bert Vogelstein Thorne et al., 2010 | N/A |
| HCT116 WTKO STF | This paper | N/A |
| MEF | Laboratory of Charles Murtaugh Barrott et al., 2011 | N/A |
| MEF PORCNKO | Laboratory of Charles Murtaugh Barrott et al., 2011 | N/A |
| L-Wnt3a | ATCC | CRL-2647 |
| L | ATCC | CRL-2648 |
| MEF Caveolin-1KO | ATCC | CRL-2753 |
| MEF LRP6flox | Laboratory of Bart Williams Zhong et al., 2012 | N/A |
| 293FT | Laboratory of David Carbone | N/A |
| HEK293-CMV | Thorne et al., 2010 | N/A |
| HEK293 DVL TKO | Laboratory of Stephane Angers Gammons et al., 2016 | N/A |
| Experimental Models: Organisms/Strains | | |
| Mouse: C57BL/6J-ApcMin/J | The Jackson Laboratory | Stock # 002020 |
| D. melanogaster: Apc1 RNAi | Vienna Drosophila Resource Center | #51469 |
| D. melanogaster: Arri1 RNAi | Vienna Drosophila Resource Center | #4819 |
| D. melanogaster: Arri2 RNAi | Vienna Drosophila Resource Center | #6707 |
| D. melanogaster: Arri4 RNAi | Vienna Drosophila Resource Center | #6708 |
| D. melanogaster: Arri3 RNAi | Bloomington Drosophila Stock Center | #53342 |
| D. melanogaster: $Apc1^{Q8}$ | Ahmed et al., 1998 | N/A |
| D. melanogaster: wgi1 RNAi | Vienna Drosophila Resource Center | #104579 |
| D. melanogaster: wgi2 RNAi | Vienna Drosophila Resource Center | #13351 |
| D. melanogaster: wls RNAi | Vienna Drosophila Resource Center | #101700 |

(*Continued on next page*)

*Continued*

| REAGENT or RESOURCE | SOURCE | IDENTIFIER |
|---|---|---|
| D. melanogaster: y RNAi | Bloomington Drosophila Stock Center | #64527 |
| D. melanogaster: Nkd-lacZ | Zeng et al., 2000 | N/A |
| D. melanogaster: dshi1 RNAi | Bloomington Drosophila Stock Center | #31306 |
| D. melanogaster: dshi2 RNAi | Vienna Drosophila Resource Center | #101525 |
| Oligonucleotides | | |
| See Table S2 | N/A | N/A |
| Recombinant DNA | | |
| pPGK mWnt3a | Laboratory of Karl Willert<br>Willert et al., 2003 | N/A |
| pMD2.G | Laboratory of David Carbone | N/A |
| pCMVdR7.74psPAX2 | Laboratory of David Carbone | N/A |
| lentiviral TOPflash | Laboratory of David Carbone | N/A |
| pUMVC | Laboratory of Ian Macara | N/A |
| pBabe 9myc-TIR1 | Laboratory of Ian Macara<br>Holland et al., 2012 | N/A |
| pCS2+ Fz1-ER | Kaykas et al., 2004 | Addgene plasmid # 16816 |
| pCS2 Xdd1 | Wallingford et al., 2000 | Addgene plasmid # 15491 |
| pcDNA3.1 K44A HA-Dynamin1 | This paper | Addgene plasmid # 34683 |
| pCas-Guide-EF1a-GFP | OriGene | Cat# GE100018 |
| pCS2+ MT-APCT | This paper | N/A |
| pCS2+ AID-Myc-mCherry-APCT | This paper | N/A |
| pCS2+ LRP6-eYFP | This paper | N/A |
| pCIG mCherry-IRES-Cre | Laboratory of Guoqiang Gu | N/A |
| pCS2 DKK1 | Laboratory of Xi He<br>Semënov et al., 2001 | N/A |
| pMAL LRP6 (589-1244) | This paper | N/A |
| Software and Algorithms | | |
| ImageJ/FIJI | NIH | https://fiji.sc/ |
| Prism 5 | GraphPad | https://www.graphpad.com/scientific-software/prism/ |
| Other | | |
| Lipofectamine 3000 | ThermoFisher | Cat# L3000015 |
| FuGene HD | Promega | Cat# E2311 |
| DharmaFECT 1 | GE Lifesciences | Cat# T-2001 |
| DharmaFECT 2 | GE Lifesciences | Cat# T-2002 |
| HiPerfect | QIAGEN | Cat# 301705 |
| Amylose resin | New England BioLabs | Cat# E8021L |

## CONTACT FOR REAGENT AND RESOURCE SHARING

Further information and requests for resources and reagents should be directed to and will be fulfilled by the Lead Contact, Ethan Lee (ethan.lee@vanderbilt.edu).

## EXPERIMENTAL MODEL AND SUBJECT DETAILS

### Cell Lines

The following cells were generous gifts: HEK293 STF (J. Nathans, Johns Hopkins University), RPE (I. Kaverina, Vanderbilt University), MEF and MEF PORCN$^{KO}$ (C. Murtaugh, University of Utah), 293FT (D. Carbone, Ohio State University), HEK293T Dvl TKO (S. Angers, University of Toronto), HCT116 WT KO (B. Vogelstein, Johns Hopkins University), and MEF LRP6$^{flox}$ (B. Williams, Van Andel Institute). HEK293, RKO, SW480, DLD1, L-Wnt3a, L-cells, and MEF Caveolin-1$^{KO}$ were purchased from the American Type Culture Collection.

HEK293 CMV-luc was reported previously (Thorne et al., 2010). Cell lines were maintained in DMEM except for SW480 and DLD1 cells (RPMI) and HCT116 (McCoy's) with 10% FBS and 1% penicillin/streptomycin at 37°C in 5% $CO_2$.

HEK293 cells were derived from human embryonic kidney cells obtained from a healthy fetus. RPE (hTERT-RPE1) cells were isolated from a 1-year-old female donor (Rambhatla et al., 2002). DLD1 cells were obtained from a 45-year-old male donor. HCT116 cells were obtained from a 48-year-old male donor. SW480 cells were obtained from a 50-year-old male donor (Ahmed et al., 2013). L cells were obtained from 100-day old male mice. MEF Caveolin-1$^{KO}$ cells were obtained from E13.5 mouse embryos. RKO, MEF, MEF PORCN$^{KO}$, and MEF LRP6$^{flox}$ cells were described previously (Ahmed et al., 2013; Barrott et al., 2011; Zhong et al., 2012).

### Three-Dimensional Organoid Culture

Organoids from isolated polyps of *APC$^{min}$* mice were prepared as previously described (Li et al., 2017). Jejunum from ~8-week-old *APC$^{min}$* mice (*C57BL/6J-Apc$^{Min}$/J*) was obtained and washed with phosphate-buffered saline (PBS) followed by incubation for 20 min with cold PBS containing 1.5 mM dithiothreitol and 30 mM EDTA. Tissue was then incubated with warm PBS containing 15 mM EDTA for 6 min, vigorously shaken to release intestinal crypts, and centrifuged. The resulting crypt pellet was washed with 30X volume of basal media (Dulbecco's modified Eagle media/F12 plus 2 mM GlutaMAX, 10 mM Hepes, penicillin/streptomycin (100 U/mL), and 1X N2 and 1X B27 supplements). Purified crypts were filtered with a 100 μm cell strainer and embedded in Matrigel (Corning). Isolated organoids were maintained in basal media supplemented with niche factors (epidermal growth factor (50ng/mL), R-spondin1 (250ng/mL), Noggin (100ng/mL), and 1mM Jagged-1) with or without Wnt3a (using 25% L-WRN conditioned media (Miyoshi and Stappenbeck, 2013)) and Pitstop-2 or mAb7E5 for 4 days. All experiment procedures were carried out in accordance with recommendations in the *Guide for the Care and Use of Laboratory Animals* of the National Institutes of Health and with the policies of the University of Miami IACUC.

### Drosophila Stocks

RNAi lines were expressed in progenitor cells using temperature-sensitive progenitor cell driver *esg$^{ts}$* (*UAS-dicer2; esg-gal4 tubgal80$^{ts}$ UAS-GFP/CyO*) (Guo et al., 2013; Micchelli and Perrimon, 2006):

*Apc1* RNAi (Vienna Drosophila Resource Center [VDRC] #51469), *arr* RNAi lines (*arr$^{i1}$*, VDRC#4819; *arr$^{i2}$*, VDRC #6707; *arr$^{i3}$*, Bloomington Drosophila Stock Center [BDSC] #53342 and *arr$^{i4}$*, VDRC #6708), *dsh* RNAi lines (*dsh$^{i1}$*, BDSC #31306; *dsh$^{i2}$*, VDRC #101525), *wg* RNAi lines (*wg$^{i1}$*, VDRC #104579; *wg$^{i2}$*, VDRC #13351), *wls* RNAi (VDRC #103812) and *y* RNAi (BDSC #64527).

*Nkd-lacZ* (Zeng et al., 2000) was used as Wg target gene reporter.

*Apc1$^{Q8}$* (Ahmed et al., 1998) was used as a null allele.

## METHOD DETAILS

### Transfections

Plasmid transfections were performed using $CaCl_2$, Lipofectamine 3000 (Invitrogen), or FuGene HD (PROMEGA). $CaCl_2$ transfections were performed as follow: cells were seeded at 50%-60% confluency in 6-well plates and incubated overnight. To transfect an individual well: 1μg of DNA was mixed with 6.1μl of $CaCl_2$ and sterile water for a final concentration of 100 μl, and added to a tube containing 100 μl of 2X HBS (280 mM NaCl, 10mM KCl, 1.5mM $Na_2HPO_4$-$2H_2O$, 12mM Dextrose (D-Glucose), and 50mM HEPES). Mixed by bubbling air and added dropwise to the cells. Lipofectamine 3000 and FuGene transfections according to manufacturer's protocol. siRNA transfections were performed using Dharmafect1 (HEK293 and RKO cells), Dharmafect2 (SW480, DLD1, and HCT116 cells) (both from Dharmacon), or HiPerfect (RPE cells) (Qiagen) according to manufacturer's protocol. siRNAs were transfected in a pool consisting of two distinct siRNAs in all experiments except where noted.

### Immunoblots and Immunoprecipitation

Whole cell lysates were obtained using non-denaturing lysis buffer (NDLB) (50 mM Tris-Cl (pH 7.4), 300 mM NaCl, 5 mM EDTA, 1% (w/v) Triton X-100, 1 mM PMSF, 1 mM sodium orthovandate, 10 mM NaF, and phosphatase inhibitor cocktail (Roche)). Soluble fractions were prepared for immunoblotting. Cytoplasmic fractionation was performed as previously described (Thorne et al., 2010). Cells were incubated on ice in lysis buffer (10 mM HEPES (pH 7.8), 10 mM KCl, 2 mM $MgCl_2$, 0.1 mM EDTA, 1 mM PMSF, 1 mM sodium orthovandate, 10 mM NaF, and phosphatase inhibitor cocktail (Roche)), scraped, transferred to microfuge tubes, and NP-40 was added to 0.5%. Lysates were vortexed and sheared 8 times using a 23-gauge needle. Lysates were centrifuged at 16,000Xg for 2 min. Supernatants (cytoplasmic fractions) were recovered. For co-immunoprecipitations, cell lysates were prepared using NDLB. Lysates were diluted to 1 mg/mL and incubated with antibody for 1 h in a TOMY shaker at 4°C followed by addition of Protein G magnetic beads (New England Biolabs) for 1 h. Beads were washed 3 times with 10X volumes of NDLB. Proteins were eluted from beads with protein sample buffer and analyzed by SDS-PAGE and immunoblotting. Chemiluminescence signal was detected using a C-DiGit blot scanner (LI-COR).

### Generation of the mAb7E5 Antibody

A cDNA fragment corresponding to the extracellular domain of human LRP6 (amino acids 589-1244) was cloned into the pMAL vector (NEB) and transformed into BL21(DE3) cells (Invitrogen). Briefly, cells were grown in LB and induced with 300 μM IPTG for 4 h at room

temperature. Cells were then centrifuged at 2,500 RPM for 30 min. Pellets were re-suspended in Buffer A (50 mM Tris pH 8.0, 200 mM NaCl, 0.1% Tween-20 and 1 mM PMSF), sonicated, and centrifuged at 12,000 RPM for 30 min. The supernatant was then incubated with amylose resin (NEB) for 2 h with rocking at 4°C. Resin was washed 2X with Buffer A, 1X with Buffer B (50 mM Tris pH 8.0, 50 mM NaCl, and 1 mM PMSF), and bound proteins eluted with 1% maltose in Buffer B. The purified protein was used to inoculate BALB/c mice for monoclonal antibody production by the Vanderbilt Protein and Antibody Core. Fusion clones (1,500) were initially screened based on their capacity to bind the antigen as assessed by ELISA. Of these clones, eight were found to inhibit Wnt3a-stimulated signaling in HEK293 STF cells but not endogenous Wnt signaling in the colorectal cancer cell line, SW480. Four additional clones were found to inhibit Wnt3a-induced signaling in HEK293 STF cells as well as endogenous Wnt signaling in SW480 cells. Of these four clones, mAb7E5 was found to be the most potent in both cell lines and was chosen for further characterization.

### Generation of RKO APC$^{KO}$

Two APC gRNA sequences (5'-CCCCCTATGTACGCCTCCC-3' and 5'-CTTTGACAAACTTGACTTT-3') were cloned into pCAS-Guide-eGFP (Origene) using BamHI and BsmBI. APC gRNA oligos were designed with a 5'-GATCG overhang and extra guanidine nucleotide on the 3'-end (Sigma). Oligonucleotides were annealed as per manufacturer's protocol using a 4-step PCR procedure. Digested pCAS-Guide-eGFP vector was ligated to the annealed oligos using T4 ligase. Final clones were sequence-verified. Plasmids containing the two APC gRNA sequences were transfected into RKO cells at 80% confluence using Fugene HD. Transfected cells were sorted by flow cytometry (Vanderbilt Flow Cytometry Core) as single cells into a 96-well plate. Single colonies were grown to confluence and split into 24-well plates. Clones were propagated and screened by TOPflash. Clones showing activation compared to vector control were screened by immunofluorescence and stained for β-catenin. Clones with high β-catenin levels were further screened by immunoblotting.

### Generation of Stable Cell Lines

To obtain lentivirus, 293FT cells were seeded at 1.2x10$^6$ on 60mm dish in 3 mL of DMEM, 10% FBS, without antibiotic. The next day, cells were transfected with 6.6μg lentiviral DNA contruct (lentiviral TOPflash, pLKO.1 APCshRNA, or pBabe TIR1-9myc), with 5μg psPAX2 (or puMVC for pBabe 9myc-TIR1), 2μg pMD2.G, 21μl 2MCaCl$_2$, and sterile water (for a final volume of 170μL), mixed with 170μΛ 2X HBS by bubbling air through the mixture. Cells were incubated with 25mM Chloroquine for 0min before adding the DNA mix. After 5-7 h, the transfection media was replaced with fresh DMEM+10% FBS, and media containing lentivirus or retrovirus was harvested after 72 h.

RKO, DLD1, HCT116 WT KO, and RPE cells were incubated with 1.5 mL of TOPflash or APC shRNA lentivirus, and RKO APC$^{KO}$ cells were incubated with 1.5 mL 9myc-TIR1 retrovirus with 12 μg polybrene (hexadimethrine bromide) for 4 h. Media was removed and cells incubated for 48 h prior to selection with puromycin or G418. To generate MEF LRP6 $^{KO}$, primary MEF LRP6$^{flox}$ cells were immortalized by transfecting SV40 and selected with 500μg G418 for 1 week. Cells were then transfected with pICG mCherry-IRES-Cre, and mCherry positive cells (MEF LRP6$^{KO}$) were isolated by FACS.

### Sucrose Density Gradients

Lysates from RKO, RKO incubated for 2 h with 20 ng recombinant Wnt3a (Times Bioscience), and RKO APC$^{KO}$ were prepared using NDLB as described in the *Immunoblots and immunoprecipitation* section. Lysates and MW standards (BioRad) were layered on top of sucrose gradients containing equal volumes of 5%, 10%, 20%, and 30% sucrose in PBS (137 mM NaCl, 7 mM $Na_2HPO_4$, and 3 mM $NaH_2PO_4$, pH 7.2). Gradients were centrifuged for 4 h at 46,000 rpm in a SW55Ti swinging-bucket rotor (Beckman Coulter). Fractions were collected, precipitated using a protein precipitation kit (National Diagnostics) according to manufacturer's protocol, resuspended in 6X Sample Buffer, and analyzed by immunoblotting.

### Endocytosis Assays

Cells were plated in four 35 mm dishes and incubated at 37°C with L-cell conditioned media (L CM), Wnt3a Conditioned Media (Wnt3a CM) or 20 ng/mL recombinant Wnt3a (Time Bioscience), 30 mM LiCl, or 2 μM CHIR-99021 for 24 h. Cells were then incubated at 4°C for 3 h. Cells were lysed in NDLB at 0, 1, 2, and 3 h post temperature shift. For recovery assays, dishes were then shifted back to 37°C, and lysates were taken at 0, 1, 2, and 3 h. For small molecule experiments, cells were preincubated for 30 min with chloroquine, pitstop-2, or nystatin as indicated, incubated with 20 ng/mL recombinant Wnt3a (Time Bioscience) for 2 h, and either analyzed by confocal microscopy or washed with ice cold PBS and lysed with NDLB.

### Microscopy

For β-catenin staining, cells were fixed in methanol at -20°C, washed in TBS plus 0.1% Triton X-100, blocked in Abdil buffer (TBS, 0.1% Triton X-100, 2% BSA, and 0.1% sodium azide) overnight at 4°C, washed with TBS plus 0.1% Triton X-100, and incubated with anti-β-catenin antibody (1:500, Vanderbilt Protein and Antibody Resource). Cells were incubated with Alexa Fluor 488-conjugated anti-mouse secondary antibody (1:1000) and mounted in ProLong Gold Antifade Reagent with DAPI (Invitrogen). Images were acquired using a CoolSNAP ES camera mounted on a Nikon Eclipse 80i fluorescence microscope with 40X and 60X objectives. For immunostaining of APC, clathrin, and caveolin-1, RPE cells were seeded on 12 mm glass coverslips, cultured for 24 h, left untreated or treated with Wnt3a ligand (20 ng/mL), incubated in tissue culture media for an additional 2 h, fixed at 37°C for 20 min in 4% paraformaldehyde in PBS, rinsed 3X with 100 mM glycine in PBS, and incubated in 0.1% Triton X-100 in PBS

with 5% glycine and 5% goat serum for 1 h at room temperature. Cells were incubated with mouse anti-APC antibody (Santa Cruz) plus rabbit anti-clathrin heavy chain monoclonal antibody (1:200, Cell Signaling) or rabbit anti-caveolin-1 polyclonal antibody (1:200, BD Transduction Laboratories) in blocking buffer with 0.05% Tx-100 for 2 h at room temperature, rinsed with PBS, incubated for 1 h in Alexa Fluor 488- and Alexa Fluor 546-conjugated secondary antibodies (1:300), and washed in PBS. Coverslips were mounted on glass slides with Prolong Gold Antifade Reagent. For Golgi immunostaining, RKO APC$^{KO}$ TIR1 cells were incubated with Brefeldin A (5μg; Sigma) or DMSO as indicated and fixed as described above. Cells were immunostained using anti-Giantin (1:200, Abcam) and DRAQ5 (Thermo Fisher). Fluorescent images were acquired using a Zeiss LSM 510 confocal microscope (Carl Zeiss Microscopy, Inc.; Thornwood, NY) with a Plan-Apochromat 100X/1.4 oil Neofluar oil immersion objective and Argon/2 30 mW laser (458, 488, 514 nm) or HeNe lasers (543 or 633 nm).

### Live Cell Imaging

Cells were plated in 35 mm glass bottom dishes (MatTek Corporation) at ~50% confluency and transfected with LRP6-eYFP for 6 h. Media was replaced by red phenol-free DMEM + 10% FBS. Cells were pre-incubated for 30 min with small molecules or mAb7E5 and/or incubated with 20 ng recombinant Wnt3a for 2 h. For time-lapse live cell imaging one control stack was taken of 7-10 cells using "mark and find" (Leica Application Suite). Wnt3a was added to the MatTek dish, refocusing was done, and subsequent z-stacks of the same cells were taken every 9 min for 3 h. Imaging was performed on a Leica SP5 confocal microscope using the Live Cell Controller by Live Cell at 37°C and 85-90% relative humidity. The 561 nm laser was used for excitation, and the laser power remained the same during acquisition for each experiment. This eliminated cells not visible under a certain threshold of brightness to account for heterogeneity in plasmid expression of transiently transfected plasmids.

### Organoid Lentiviral Transduction

Lentivirus was packaged in HEK293T cells using pMD2.G and psPAX2 vectors and either the GIPZ Non-silencing Lentiviral shRNA control vector (Dharmacon, RHS4346) or two pooled GIPZ shLRP6 vectors (V3LMM_484540 and V3LMM_484536). 30 mL of lentiviral supernatant was harvested, filtered through a 0.45 mm filter, and concentrated overnight via centrifugation at 8,000Xg. The lentiviral pellet was resuspended in 250 μL L-WRN media with 8 mg/mL polybrene and 10 mM Y27632. *APC$^{min}$* organoids were collected and Matrigel-digested for 30 min on ice using Cell Recovery Solution (Corning). Organoids were pelleted at 150Xg for 5 minutes then re-suspended in 1 mL cold PBS and sheared through a 25G needle 1X. Dissociated organoids were pelleted, resuspended in 250 mL concentrated lentivirus, spinoculated at 600 X g for 1 h at 32°C, incubated at 37°C for an additional 6 h, pelleted, resuspended in Matrigel, plated in 12-well plates, and overlayed with 0.5 mL basal media for 4 days.

### Organoid Immunofluorescence

*APC$^{min}$* organoids were fixed in 4% formaldehyde in PBS for 30 min to 1 h at room temperature in 1.5 mL tubes, permeabilized with 0.5% Triton X-100 in TBS for 30 min at room temperature, incubated overnight at 4°C in blocking buffer (PBS, 1% BSA, 3% normal goat serum, 0.2% Triton X-100), followed by overnight incubation at 4°C in blocking buffer with mouse anti-β-catenin antibody (1:500, Vanderbilt Protein and Antibody Resource). Organoids were then washed 3X for at least 30 min in 0.1% Triton X-100 in TBS and incubated 2-3 h at room temperature in blocking buffer with Cy3-conjugated anti-mouse secondary antibody (1:500, Jackson Immuno). Stained organoids were incubated with Hoescht (1:1000) in TBS for 15 min at room temperature and mounted in Mattek dishes with ProLong Gold Antifade Reagent (Invitrogen). Imaging was done using a Nikon Spinning Disk microscope with Andor DU-897 EMCCD camera and 561 nm and 405 nm lasers.

### Drosophila RNAi Experiments

Temporal RNAi-mediated knockdown in progenitor cells was performed using the temperature-sensitive progenitor cell driver *esg$^{ts}$*. For concomitant *Apc1* and *arr* knockdown, crosses were maintained at 18°C until late third instar larval stage then shifted to 29°C restrictive temperature to allow RNAi-mediated knockdown during pupation. For concomitant *Apc1* and *dsh* knockdown, crosses were maintained at 18°C until second instar larval stage then shifted to 29°C.

To induce knockdown of *arr*, *dsh*, *wg*, and *wls* in an *Apc1$^{Q8}$* background, crosses were maintained at 18°C until late third instar larval stage then shifted to 29°C restrictive temperature. Expression of the Wg target gene reporter *nkd-lacZ* was analyzed in *Apc1$^{Q8}$* mutants with and without expression of *arr* and *dsh* RNAi.

Genotype for arrow knockdown in Apc1 null mutant (Figure 8): esg-Gal4 tubGal80$^{ts}$ UAS-GFP/ UAS-arrow RNAi; Apc1$^{Q8}$

Genotype for dsh knockdown in Apc1 null mutant (Figure 8): esg-Gal4 tubGal80$^{ts}$ UAS-GFP/ UAS-dsh RNAi; Apc1$^{Q8}$

Genotype for simultaneous knockdown of arrow and Apc1 (Figure S7): UAS-dicer2/+; esg-Gal4 tubGal80$^{ts}$ UAS-GFP/+ or UAS-arrow RNAi; UAS-Apc1 RNAi/UAS-arrow RNAi or +.

Genotype for simultaneous knockdown of dsh and Apc1 (Figure S7): UAS-dicer2/+; esg-Gal4 tubGal80$^{ts}$ UAS-GFP/+ or UAS-dsh RNAi; UAS-Apc1 RNAi/UAS-dsh RNAi or +.

Genotype for arrow knockdown in Apc1 null mutant expressing nkd-lacZ (Figure S8): esg-Gal4 tubGal80$^{ts}$ UAS-GFP/ UAS-arrow RNAi; Apc1$^{Q8}$/ nkd-lacZ Apc1$^{Q8}$.

Genotype for dsh knockdown in Apc1 null mutant expressing nkd-lacZ (Figure S8): esg-Gal4 tubGal80$^{ts}$ UAS-GFP/ UAS-dsh RNAi; Apc1$^{Q8}$/ nkd-lacZ Apc1$^{Q8}$.

Genotype for yellow knockdown in Apc1 null mutant expressing nkd-lacZ (Figure S8): esg-Gal4 tubGal80$^{ts}$ UAS-GFP/ UAS-y RNAi; Apc1$^{Q8}$/ nkd-lacZ Apc1$^{Q8}$.

Genotype for wg knockdown in Apc1 null mutant (Figure 8): esg-Gal4 tubGal80$^{ts}$ UAS-GFP/ UAS-wg RNAi; Apc1$^{Q8}$

Genotype for wls knockdown in Apc1 null mutant (Figure 8): esg-Gal4 tubGal80$^{ts}$ UAS-GFP/ UAS-wls RNAi; Apc1$^{Q8}$

### Drosophila Immunohistochemistry

Adult intestines (2 d) were dissected in PBS, fixed in 4% paraformaldehyde in PBS for 45 min, washed in PBS plus 0.1% Triton X-100, incubated in PBS plus 0.1% Tween-20 and 10% BSA for 1 h at room temperature, and incubated at 4°C overnight in PBS plus 0.5% Triton X-100 with chicken anti-GFP antibody (1:10000, Abcam), mouse anti-β-gal (Promega, 1:500), mouse anti-Arm (Developmental Studies Hybridoma Bank, [DSHB], 1:20), and mouse anti-Prospero (DSHB, 1:100). Samples were stained with secondary antibody (goat anti-chicken Alexa Fluor 488 and anti-mouse Alexa Fluor 555 conjugates; ThermoFisher Scientific, 1:500) for 2 h at room temperature, stained with DAPI (2 μg/mL), and mounted in Prolong Gold (Invitrogen). Confocal images were obtained from the R4 region of the posterior midgut with a Nikon A1RSi confocal microscope with 60X lens, and the number of *esg*-positive cells in a field of 0.051 mm$^2$ was counted (>15 posterior midguts analyzed per genotype). Images were processed using Adobe Photoshop software. The intensity of *nkd-lacZ* expression along a line drawn across the posterior midgut was quantified using NIS-Elements software (Nikon) from images obtained with a 20X lens. The distance between the start of *nkd-lacZ* expression at the hindgut/midgut boundary and the last peak of high intensity *nkd-lacZ* expression in the posterior midgut was measured.

### Auxin-Dependent Degradation Assay

RKO APC$^{KO}$ TIR1 cells were plated in 35 mm dishes and transfected with pCS2 Myc-APC$^{T}$ or pCS2 AID-Myc-mCherry-APC$^{T}$. At 24 h post-transfection, cells were incubated with 500 μM auxin analog 1-Naphthaleneacetic acid (Sigma). For Brefeldin A experiments, cells were pre-incubated with 5 μg Brefeldin A or DMSO before addition of auxin. Timepoints were taken every 30 min for 2 h. Cells were lysed in NDLB and immunoblotted.

### Reporter Assay

For cell-based luciferase assays, HEK293 STF, RKO STF, SW480 STF, DLD1 STF, HCT116 STF, HCT116 WT KO STF, and HEK293 CMV-Luc cells were seeded into 24-well plates at ~50% confluency. Cells were incubated with L CM, Wnt3a CM, 20 ng/mL purified Wnt3a (Time Bioscience), or 30 mM LiCl prior to lysis with 1X Passive Lysis buffer (Promega). Luciferase expression was measured using Steady-Glo Luciferase Assay (Promega). For inhibitor studies, cells were incubated with mAb7E5, Wnt-C59 (Cellagen Technology), IWP-2 (StemRD) or Fz8-Fc (R&D Systems) for 24 h (or 48 h for SW480, DLD1, and HCT116 cells) prior to lysis. Luciferase signal was normalized to viable cell number using CellTiter-Glo Assay (Promega). Alternatively, TOPflash experiments in HEK293, HEK293 Dvl TKO, MEF, MEF PORCN$^{KO}$, MEF Caveolin-1$^{KO}$, RKO, and RKO APC$^{KO}$ cells were performed as follows. Cells were plated, co-transfected with TOPflash and Renilla expression plasmids at 24 h, and lysed using Dual-Glo Assay (Promega) 24 h later. Luciferase signal was normalized to co-transfected Renilla expression. Data were normalized to the signal obtained from positive controls (plotted as 100% activation). Assays were performed in quadruplicate and repeated at least 3X.

### RNA Isolation and qRT-PCR

HEK293 cells were treated with LRP6 siRNA and APC siRNA for 72 h, harvested using STAT60 reagent (Amsbio) according to manufacturer's protocol, and further purified using RNeasy purification kit (Qiagen). RNA (2 μg) was reverse transcribed to cDNA using High-Capacity cDNA Reverse Transcription Kit (Thermo Scientific). qRT-PCR was performed on a Bio-Rad C1000 thermocycler using predesigned and revalidated TaqMan probes that span exons (Thermo Scientific). GAPDH was used as reference control. Technical duplicates were performed for each gene.

## QUANTIFICATION AND STATISTICAL ANALYSIS

### Immunoblotting Quantification

Chemiluminescence signal from immunoblots were detected using a C-DiGit blot scanner (LI-COR). Obtained images and band intensity were analyzed using Image Studio (LI-COR).

### Line Scan Analysis

Images or maximum-intensity projections of z-stacks were analyzed using ImageJ/FIJI (National Institutes of Health, Bethesda, MD). Line scan analyses to quantify nuclear β-catenin or LRP6-eYFP signal intensity were performed using ImageJ. At least five representative cells were measured per condition.

### Organoid Measurement

To measure organoid size, a straight line was drawn across the diameter of *APC$^{min}$* organoids. The number of pixels were quantified and normalized to untreated control. At least 20 organoids per condition were analyzed. All measurements were performed using Image J/FIJI (National Institutes of Health, Bethesda, MD).

### Statistical Analysis

All graphs were generated using Prism (GraphPad Software, Inc.). Statistical analyses were performed using a two-tailed, unpaired Student's t-test, except for colocalization analyses. A value of $p<0.05$ is considered statistically significant.

### Colocalization Analysis

For colocalization analysis, Intensity Correlation Analysis plugin in FIJI was used. Pearson's correlation coefficients were calculated using 4X zoom images. For each condition, 10-19 images were analyzed. Box and whisker plots were used for reporting Pearson's correlation coefficients. A two-tailed, unpaired, non-parametric Mann-Whitney U-test was used for calculating p-values.